Available online at www.sciencedirect.com

SciVerse ScienceDirect

Geochimica et Cosmochimica Acta 99 (2012) 128–145

Geochimica et Cosmochimica Acta

www.elsevier.com/locate/gca

Factors controlling the silicon isotope distribution in waters and surface sediments of the Peruvian coastal upwelling

Claudia Ehlert [a,*], Patricia Grasse [a,*], Elfi Mollier-Vogel [b], Tebke Böschen [a], Jasmin Franz [a], Gregory F. de Souza [c,1], Ben C. Reynolds [c], Lothar Stramma [a], Martin Frank [a]

[a] Helmholtz Centre for Ocean Research Kiel (GEOMAR), Kiel, Germany
[b] Institute of Geosciences, University of Kiel, Germany
[c] Institute of Geochemistry and Petrology, ETH Zurich, Switzerland

Received 14 June 2012; accepted in revised form 23 September 2012; Available online 29 September 2012

Abstract

We present the first systematic study of the silicon isotope composition in the water column ($\delta^{30}Si_{Si(OH)_4}$) and in diatoms ($\delta^{30}Si_{diatom}$) from the underlying surface sediments in a coastal upwelling region. The surface waters upwelling on the shelf off Peru are mainly fed by southward flowing subsurface waters along the coast, which show a mean $\delta^{30}Si_{Si(OH)_4}$ of +1.5‰. The concentration of dissolved silicic acid ($Si(OH)_4$) increases towards the south in these waters and with increasing water depth, suggesting lateral mixing with water masses from the south and intense remineralisation of particulate biogenic silica ($bSiO_2$) in the water column and in the surface sediments. Surface waters in the realm of the most intense upwelling between 5°S and 15°S have only marginally elevated $\delta^{30}Si_{Si(OH)_4}$ values ($\delta^{30}Si_{Si(OH)_4} = +1.7‰$) with respect to the source Si isotope composition, whereas further north and south, where upwelling is less pronounced, surface waters are more strongly fractionated ($\delta^{30}Si_{Si(OH)_4}$ up to +2.8‰) due to the stronger utilisation of the smaller amounts of available $Si(OH)_4$. The degree of $Si(OH)_4$ utilisation in the surface waters along the shelf estimated from the $Si(OH)_4$ concentration data ranges from 51% to 93%.

The $\delta^{30}Si_{diatom}$ values of hand-picked diatoms in the underlying surface sediments vary from +0.6‰ to +2.0‰, which is within the range of the expected fractionation between surface waters and diatoms. The fractionation signal in the surface waters produced during formation of the diatoms is reflected by the $\delta^{30}Si_{diatom}$ values in the underlying sediments, with the lowest $\delta^{30}Si_{diatom}$ values in the main upwelling region. The silicon isotope compositions of $bSiO_2$ ($\delta^{30}Si_{bSiO_2}$) from the same surface sediment samples are generally much lower than the $\delta^{30}Si_{diatom}$ signatures indicating a significant contamination of the $bSiO_2$ with biogenic siliceous material other than diatoms, such as sponge spicules. This shift towards lighter $\delta^{30}Si_{bSiO_2}$ values by up to −1.3‰ compared to $\delta^{30}Si_{diatom}$ signatures for the same surface sediment samples potentially biases the interpretation of $\delta^{30}Si$ paleorecords from sediments with low $bSiO_2$ concentrations, and thus the reconstruction of past $Si(OH)_4$ utilisation in surface waters.

1. INTRODUCTION

The Peruvian coastal upwelling region is characterised by extremely high rates of primary productivity (Thiede and Suess, 1983; Berger et al., 1989; Pennington et al., 2006). Persistent easterly trade and alongshore winds produce offshore Ekman transport of surface water, which is replaced by upwelled, nutrient-rich subsurface waters. The

* Corresponding authors. Address: Helmholtz Centre for Ocean Research Kiel (GEOMAR), Wischhofstr. 1–3, 24148 Kiel, Germany. Tel.: +49 0431 600 2571; fax: +49 0431 600 2925 (C. Ehlert), tel.: +49 0431 600 2507; fax: +49 0431 600 2925 (P. Grasse).

E-mail addresses: cehlert@geomar.de (C. Ehlert), pgrasse@geomar.de (P. Grasse).

[1] Current address: Program in Atmospheric and Oceanic Sciences, Princeton University, USA.

0016-7037/$ - see front matter © 2012 Elsevier Ltd. All rights reserved.
http://dx.doi.org/10.1016/j.gca.2012.09.038

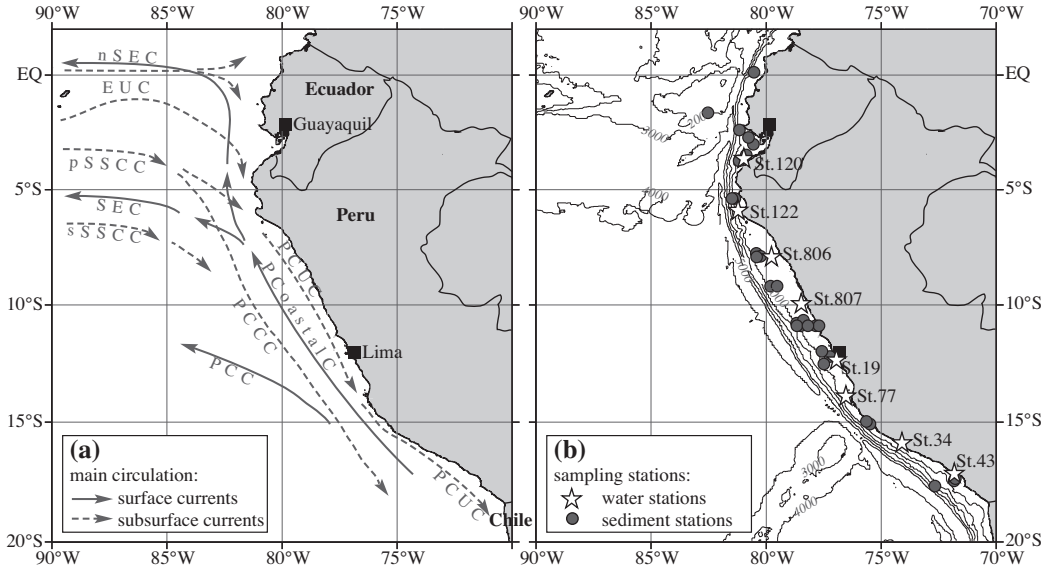

Fig. 1. Maps showing the (a) generalised circulation pathways of currents influencing the near-coastal areas (after Ayón et al., 2008; Kessler, 2006; Penven et al., 2005; and ADCP data according to Czeschel et al., 2011). Surface currents (solid line): (n)SEC (northern) South Equatorial Current, PCC Peru–Chile Current, PCoastalC Peru Coastal Current, subsurface currents (dashed line): EUC Equatorial Undercurrent, pSSCC and sSSCC primary and secondary Southern Subsurface Countercurrent, PCUC Peru–Chile Undercurrent, PCCC Peru Chile Countercurrent. (b) Location of the CTD-rosette stations (white stars with station numbers) and surface sediment stations (grey dots). The bathymetry is given for 0 to 5000 m water depth in 1000 m increments.

main water masses supplying the Peruvian upwelling system are the southward flowing Peru–Chile Countercurrent (PCCC) and the Peru–Chile Undercurrent (PCUC) (Brink et al., 1983; Toggweiler et al., 1991), which prevails between 50 and 150 m water depth, as well as the northward flowing Peru Coastal Current (PCoastalC) (Huyer et al., 1987; Karstensen and Ulloa, 2008). The PCCC and the PCUC currents are partly fed by the eastward flowing high salinity and oxygen enriched waters of the Equatorial Undercurrent (EUC) (Lukas, 1986; Penven et al., 2005; Kessler, 2006) and the Southern Subsurface Countercurrents (SSCC) (Fig. 1a). Upwelling intensity is generally high during most of the year with its maximum during austral winter (Gunther, 1936; Strub et al., 1998), which results in year-round high nutrient concentrations in the surface waters (Pennington et al., 2006). Primary productivity, which is generally dominated by diatoms (Estrada and Blasco, 1985; Bruland et al., 2005; Abrantes et al., 2007), is most intense during austral summer (Chavez, 1995). Upwelling and productivity are usually strongest between 10° and 15°S and decrease towards the north and south, whereas during the sampling period for this study (see Section 2) they were high between 5°S and 15°S (indicated by lowest sea surface temperatures (SSTs), highest chlorophyll *a* and silicic acid ($Si(OH)_4$) in that area, Fig. 2). The amount of primary productivity off Peru is so high that the associated decomposition of sinking organic matter causes one of the most pronounced oxygen minimum zones (OMZs) of the world's ocean (e.g. Karstensen et al., 2008; Fuenzalida et al., 2009). In the surface waters along the shelf region, nutrient concentrations, especially of nitrate, phosphate and iron, are very high and are not limiting for blooming diatoms (Bruland et al., 2005; Franz et al., 2012). Concentrations of $Si(OH)_4$ are lower where upwelling is weaker along the northern shelf and are highly depleted only further offshore (Fig. 2c). Therefore, it can be assumed that the availability of $Si(OH)_4$ is the dominant nutrient controlling diatom productivity (Dugdale et al., 1995).

Several studies have proposed that during the last glacial period unused $Si(OH)_4$ from the Southern Ocean was transported into the tropical upwelling areas via Subantarctic Mode Water, where it supposedly promoted enhanced diatom over coccolithophorid productivity (Silicic Acid Leakage Hypothesis, e.g. Nozaki and Yamamoto, 2001; Brzezinski et al., 2002; Matsumoto and Sarmiento, 2008). From reconstructions based on sedimentary records it has been inferred that most of the changes in shelf bottom water oxygen levels under the coastal upwelling system off Peru have been related to changes in surface water productivity and nutrient cycling (e.g. De Vries and Schrader, 1981; Schrader, 1992; Rein et al., 2005). However, the reconstruction of nutrient cycling based on the observed changes in nitrogen isotopes ($\delta^{15}N$) from downcore records in the Eastern Equatorial Pacific (e.g. Robinson et al., 2009) can be strongly influenced by factors other than utilisation, such as for example nitrogen loss during denitrification and/or anammox processes which occur under suboxic conditions (e.g. Codispoti et al., 2001; Lam et al., 2009). In contrast to the complex nitrogen cycle, the silicon cycle is relatively simple and the isotopic composition of stable silicon (expressed as $\delta^{30}Si$) is a powerful tool to investigate changes of $Si(OH)_4$ utilisation, as well as nutrient dynamics in the present and past ocean (De La Rocha et al., 1998; Brzezinski et al., 2002; Reynolds et al., 2008; Fripiat

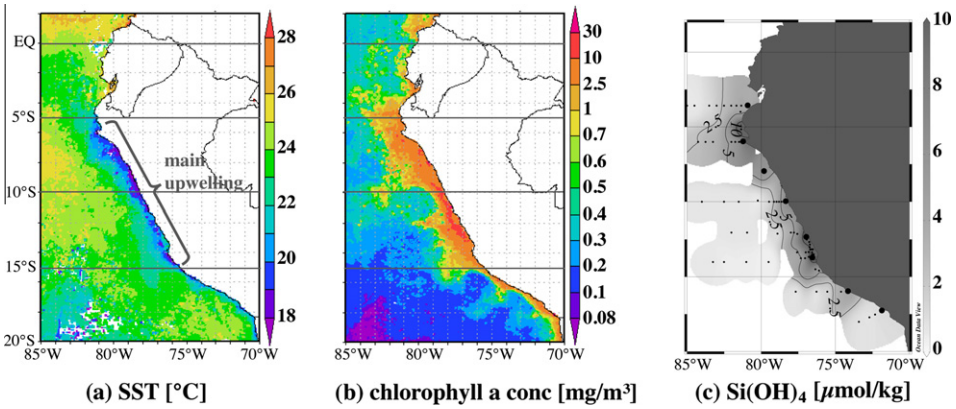

Fig. 2. Austral summer (Jan–Feb) surface water distribution of (a) SST (°C), (b) chlorophyll a concentration (mg/m^3), and (c) $Si(OH)_4$ concentration (µmol/kg, from cruises M77/3 and M77/4, small dots indicate surface water sampling locations, large dots indicate the water column stations as in Fig. 1b). Satellite data in panels (a and b) were obtained from NASA Giovanni (http://disc.sci.gsfc.nasa.gov/giovanni/overview/index.html). The bracket marks the area of the strongest upwelling between 5°S to 15°S.

et al., 2011a; de Souza et al., 2012a). Diatoms take up dissolved $Si(OH)_4$ to form their opaline frustules (Tréguer et al., 1995), a process that is associated with the fractionation of Si isotopes. The lighter isotopes are preferentially incorporated into the diatom frustules and leave the residual $Si(OH)_4$ in surface waters enriched in the heavier isotopes. The fractionation factor between seawater and diatoms is about −1.1‰ (De La Rocha et al., 1997; Milligan et al., 2004; Varela et al., 2004; Reynolds et al., 2006; Beucher et al., 2008). In areas of strong upwelling the degree of utilisation and therefore the dissolved $\delta^{30}Si_{Si(OH)_4}$ in the surface water is expected to be low due to continuous supply of large amounts of less fractionated $Si(OH)_4$ from subsurface waters. In contrast, in areas of weak upwelling the $Si(OH)_4$ in the surface waters will be almost completely utilised, which means that $\delta^{30}Si_{Si(OH)_4}$ will correspondingly be very high. The $\delta^{30}Si_{Si(OH)_4}$ distribution in surface waters should therefore likely reflect the degree of $Si(OH)_4$ utilisation from the available pool (Varela et al., 2004; Cardinal et al., 2005; Reynolds et al., 2006). Changes in $Si(OH)_4$ utilisation by diatoms due to variations in $Si(OH)_4$ supply and upwelling intensity are therefore expected to be reflected by the Si isotope composition of surface waters ($\delta^{30}Si_{Si(OH)_4}$) and correspondingly that of the diatoms growing in them, which are deposited in the surface sediments below ($\delta^{30}Si_{bSiO_2}$ for biogenic silica ($bSiO_2$) and $\delta^{30}Si_{diatom}$ for hand-picked diatoms extracted from the surface sediments).

In this study, we present for the first time water column profiles of the Si isotope composition of dissolved $Si(OH)_4$ for eight shallow water stations, together with isotopic analyses of different diatom fractions extracted from the underlying surface sediments along the Peruvian shelf between the equator and 17.5°S (Fig. 1). This range covers the major gradients of coastal upwelling intensity (Fig. 2). The goal of this study is to determine the main factors controlling the $\delta^{30}Si$ of $Si(OH)_4$ in the surface waters and how these signatures are recorded by the corresponding sedimentary diatoms as a function of lateral and vertical mixing and/or upwelling intensity and diatom productivity and ecology.

2. MATERIAL AND METHODS

All samples were collected during cruises M77/1 to M77/4 with the German RV Meteor between October 2008 and February 2009 within the framework of the Collaborative Research Centre (SFB) 754: Climate – Biogeochemistry Interactions in the Tropical Ocean. All sampling stations are located on the Ecuadorian and Peruvian shelf between the equator and 17.5°S (Fig. 1b, Tables 1 and 2).

The water samples for the whole water column, including bottom water, were collected using a rosette with 24 Niskin bottles (10 L each) equipped with a SeaBird CTD. Subsamples for $Si(OH)_4$ concentration measurements were frozen onboard immediately after sampling and were measured later at the Max-Planck Institute (MPI) for Marine Microbiology in Bremen, Germany. $Si(OH)_4$ concentrations of frozen samples were compared to selected filtered and acidified (non-frozen) seawater samples from the same Niskin bottles. The reproducibility between the data of the two methods was within 5–10% ($n = 28$) with no systematic variations. Oxygen concentrations were determined with the O_2-sensor of the CTD and were later calibrated against bottle data obtained by Winkler titration (Winkler, 1888).

Seawater samples for $\delta^{30}Si_{SiOH_4}$ analysis (500 to 2000 ml) were immediately filtered on board through nitrocellulose acetate filters (0.45 µm pore size), acidified to pH 2 with concentrated Teflon-distilled HCl (1 mL HCl per litre of seawater), and stored in acid cleaned polyethylene bottles. In the clean laboratory of GEOMAR Si was separated from the water samples using a brucite–coprecipitation method (following Reynolds et al. (2006), after Karl and Tien (1992)). Given that incomplete precipitation would lead to isotopic fractionation of the Si in the sample, recovery was checked for every sample, and only those with >97% yield were used for isotopic measurements. Depending on the $Si(OH)_4$ concentration of the samples, between 10 and 300 mL of previously neutralized seawater was precipitated at pH 10 by adding 1 M NaOH (10 µl/ml). The precipitate was dissolved in 6 M HCl resulting in a pH of 2–3. Water samples with concentrations of less than

Table 1
Seawater oxygen and $Si(OH)_4$ concentrations and $\delta^{30}Si_{Si(OH)_4}$ data from the RV Meteor cruises M77/3 and M77/4, collected in January and February 2009. $2\sigma_{sd}$ represents the external reproducibilities of repeated sample measurements.

Station	Location	Water depth (m)	Oxygen (μmol/kg)	Silicate (μmol/kg)	$\delta^{30}Si$ (‰)	$2\sigma_{sd}$
120	3°35.4′S	2.4	227.86	2.80	2.61	0.28
	80°57.0′W	4.7	227.77	2.87		
	219 m depth	10.1	221.53	2.99		
		20.5	185.57	12.40		
		30.1	116.71	14.95	1.75	0.15
		40.2	35.13	16.62		
		49.9	46.38	15.60		
		59.6	59.16	15.54	1.58	0.07
		80.4	58.31	15.54	1.76	0.11
		101.6	54.49	15.93	1.32	0.33
		120.7	35.87	18.98		
		151.2	47.16	18.37		
		151.6	48.93	18.39		
		160.3	51.28	18.29		
		170.3	50.32	18.79		
		180.4	46.76	19.18		
		217.4	20.29	22.43	1.49	0.29
122	6°00.0′S	1.9	118.82	8.97	1.86	0.09
	81°15.6′W	5.7	113.89	10.62		
	208 m depth	10.5	46.24	14.26	1.87	0.19
		19.9	5.11	16.82	1.38	0.18
		30.2	5.11	17.21		
		40.8	7.09	17.80	1.36	0.24
		51.7	7.18	18.00		
		60.6	6.23	18.88		
		69.7	5.94	20.36		
		80.2	4.90	21.15	1.48	0.14
		90.5	4.64	21.15		
		100.4	4.37	21.44		
		125.5	3.13	21.93		
		150.0	3.17	22.81		
		174.5	3.12	25.18	1.30	0.18
		198.1	3.13	26.36		
		203.2	3.20	26.16		
806	8°00.0′S	1.5	212.83	6.25	2.03	0.22
	79°50.4′W	9.7	155.43	6.95		
	146 m depth	20.8	10.72	12.16		
		30.2	6.10	14.24	1.64	0.28
		41.0	8.73	16.68		
		50.2	10.56	17.37		
		60.4	10.59	17.72	1.67	0.20
		70.6	10.43	17.72		
		81.2	9.09	18.41		
		90.2	8.39	18.76	1.62	0.28
		100.2	6.70	18.07		
		110.3	5.85	19.80		
		120.0	3.59	24.67	1.49	0.21
		129.7	2.02	30.23		
		141.0	2.12	30.92	1.58	0.35
807	10°00.0′S	2.0	65.53	9.73	1.96	0.11
	78°22.8′W	10.8	6.00	16.68		
	111 m depth	20.5	1.84	18.76		
		29.8	1.90	20.85	1.52	0.20
		39.9	1.89	23.28		
		49.6	1.91	26.06		
		60.2	1.97	26.06	1.26	0.18
		70.9	1.96	30.58		
		79.7	1.96	31.97		
		90.1	2.03	32.31	1.18	0.16

Table 1 (*continued*)

Station	Location	Water depth (m)	Oxygen (μmol/kg)	Silicate (μmol/kg)	$\delta^{30}Si$ (‰)	$2\sigma_{sd}$
		99.5	2.05	32.31		
		110.0	2.00	32.66	1.11	0.16
19	12°21.6′S	2.3	191.39	17.72	1.83	0.23
	77°00.0′W	2.7	184.47	21.20		
	100 m depth	10.4	2.08	23.50	1.63	0.20
		21.7	1.84	33.70		
		32.0	1.84	33.36		
		39.9	2.01	40.65	1.16	0.20
		51.7	1.87	39.26		
		60.2	1.98	37.53	1.42	0.19
		72.1	1.97	38.91		
		79.5	2.02	38.91	1.47	0.16
		92.0	2.02	40.65		
		97.5	2.04	41.69	1.06	0.17
77	14°00.0′S	2.0	83.46	17.54	1.71	0.31
	76°30.6′W	10.0	12.00	17.54	1.84	0.26
	199 m depth	19.2	2.64	23.92	1.57	0.29
		51.2	2.72	38.28	1.36	0.34
		150.4	2.91	32.70	1.68	0.29
		196.7	2.97	29.55	1.71	0.29
34	16°00.0′S	2.1	165.82	3.82	2.66	0.48
	74°10.8′W	11.1	158.44	4.52		
	124 m depth	20.0	132.15	7.30	1.90	0.30
		29.9	58.64	12.51		
		40.1	38.72	15.29	1.69	0.40
		50.1	25.27	20.85		
		60.2	7.72	23.98	1.75	0.22
		70.6	2.53	25.37		
		80.1	2.42	26.76	1.63	0.18
		90.4	2.12	27.80		
		100.1	2.16	29.88		
		116.9	2.35	31.62	1.26	0.22
		117.3	2.32	31.97		
43	17°18.0′S	3.9	238.46	2.14	2.81	0.33
	71°54.0′W	9.9	234.36	2.60		
	126 m depth	20.8	149.15	5.27	2.40	0.16
		30.1	81.91	10.36		
		40.0	15.15	19.33	1.49	0.18
		50.0	8.54	22.57		
		60.7	3.21	26.74	1.30	0.28
		70.3	2.17	31.01		
		80.5	2.14	32.40		
		90.3	2.15	23.07		
		97.8	2.18	30.80		
		121.0	2.28	31.23		
		121.3	2.23	31.05	1.36	0.25

~10 μmol/kg $Si(OH)_4$ were preconcentrated through additional precipitation steps applying the same method (see also Reynolds et al., 2006) to ensure that ~70 nmol Si were processed through ion-exchange chromatography.

The sediment samples were collected using a multicorer. For this study only the uppermost centimetre of each core was used. The content of $bSiO_2$ was measured following DeMaster (1981) and Müller and Schneider (1993). The extraction of diatoms from the sediment samples for Si isotope analyses followed the procedure by Morley et al. (2004). Approximately 300 μg of freeze-dried sediment was treated with concentrated H_2O_2 and HCl to remove organic matter and carbonates and subsequently wet-sieved to extract the 11–32 μm fraction. $BSiO_2$ was separated from detrital material in multiple steps using a sodium polytungstate solution with a density of 2.1–2.2 g/mL. The cleaned $bSiO_2$ samples were checked under a light microscope for residual detrital material or radiolarian remains. For dissolution of the diatom frustules the method of Reynolds et al. (2008) was applied. The samples were transferred into Teflon vials and dissolved in 1 mL 0.1 M NaOH at 130 °C for ca. 12 hours. After cooling the samples were centrifuged to separate any residual material and the supernatant was transferred into a new Teflon vial. Two hundred microlitre

Table 2
$BSiO_2$ concentration, Al/Si and Ti/Si ratios and $\delta^{30}Si$ data for $bSiO_2$ and hand-picked diatoms from surface samples from the Peruvian shelf taken during cruises M77/1 and M77/2. $2\sigma_{sd}$ represents the external reproducibilities of repeated sample measurements.

Station	Latitude	Longitude	Depth (m)	SiO2 (wt%)	$\delta^{30}Si_{bSiO_2}$	$2\sigma_{sd}$	Al/Si (mmol/mol)	Ti/Si (μmol/mol)	$\delta^{30}Si_{diatom}$	$2\sigma_{sd}$	Al/Si (mmol/mol)	Ti/Si (μmol/mol)
M772-076	00°5.5′N	80°33.4′W	290	2.81	0.75	0.29			1.77	0.10		
M772-067	01°45.1′S	82°37.5′W	2075	7.15	0.57	0.09	11.0	65.3				
M772-062	02°30.0′S	81°14.7′W	1678	5.11					1.23	0.21		
M772-071	02°50.0′S	80°50.7′W	100	2.39	−0.43	0.29	184.5	58.9				
M772-070	03°07.0′S	80°38.8′W	59	0.24	−0.10	0.13	234.6	124.6				
M772-060	03°51.1′S	81°15.5′W	701	4.28	0.53	0.22	91.9	60.2	1.82	0.40		
M772-053	05°28.9′S	81°34.0′W	2607	11.52	0.89	0.21	24.2	31.3				
M772-052	05°29.0′S	81°27.0′W	1252	8.58	0.76	0.10	80.4	83.8	1.44	0.14		
M772-047	07°52.0′S	80°31.4′W	625	3.85	0.28	0.19	61.2	59.1				
M772-050	08°01.0′S	80°30.1′W	1013	7.44	0.78	0.25	35.8	87.6	1.61	0.17		
M772-028	09°17.7′S	79°53.9′W	1105	5.01	0.30	0.10	31.2	41.5				
M772-029	09°17.7′S	79°37.1′W	437	4.64	0.65	0.28	45.3	40.1				
M772-026	10°45.1′S	78°28.4′W	424	3.62	0.10	0.14	44.1	43.9				
M772-022	10°53.2′S	78°46.4′W	1923	4.66	0.45	0.25	44.6	33.2				
M771-450	11°00.0′S	78°10.0′W	319	13.86	0.90	0.17	9.9	41.5				
M771-543	11°00.0′S	77°47.4′W	77	12.88	0.85	0.15	7.9	32.7				
M771-462	11°00.0′S	78°44.7′W	2020						1.42	0.34		
M771-460	11°00.0′S	78°35.2′W	1245	1.50	−0.10	0.29	43.9	38.1				
M771-469	11°00.1′S	77°56.6′W	145	17.62	1.03	0.15	22.4	55.4	1.05	0.38	8.0	107.2
M772-005	12°05.7′S	77°40.1‘W	214	10.94	0.95	0.10	1.1	96.0	1.76	0.31		
M771-620	12°18.6′S	77°19.2′W	150	17.65	0.92	0.18	2.3	44.8				
M771-623	12°38.2′S	77°34.6′W	1085	5.85	0.61	0.13	15.1	59.3				
M772-002	15°04.8′S	75°44.0‘W	290	20.55	1.18	0.18	10.0	47.3	0.99	0.15	6.6	103.5
M771-420	15°11.4′S	75°34.9′W	516	17.31	1.07	0.13	23.7	40.7				
M771-403	17°26.0′S	71°51.4′W	296	2.39	−0.98	0.21	45.4	84.3				
M771-396	17°26.0′S	71°51.4′W	299	6.06	0.95	0.29	27.8	102.7				
M771-407	17°34.4′S	71°56.0′W	788	2.75	0.17	0.15	40.7	77.8				
M771-411	17°47.2′S	72°44.7′W	2167	5.39	0.27	0.28	55.5	64.2	0.58	0.25	18.5	159.6

concentrated H_2O_2 (Suprapur) was added to each sample, which was then dried and redissolved in 1 mL 0.1 M NaOH at 130 °C for a few hours. Tests demonstrated that this additional step for oxidation of remaining organic matter does not affect the Si isotope results but significantly increases the stability of the beam during mass spectrometry and improves the reproducibility of the measurements. The sample solution was then diluted with 4 mL MQ water and neutralised with 0.1 mL 1 M HCl. The Si concentrations of both seawater and diatom samples were measured colorimetrically using a photospectrometer (Hansen and Koroleff, 1999).

From selected samples large diatoms were hand-picked to obtain a pure diatom $\delta^{30}Si_{diatom}$ value not influenced by any other potentially present $bSiO_2$ phases. These samples were wet sieved through a 63 μm sieve, dried and sieved into different size fractions. Between 100 and 200 individual diatom specimens (non species-specific) were hand-picked from the 125–250 μm fraction, which resulted in concentrations of about 100–150 μmol/kg Si after dissolution in 2.5 mL of solution performed with the same method as for the bulk $bSiO_2$.

Al/Si and Ti/Si ratios were measured on aliquots of most of the dissolved $bSiO_2$ and on selected hand-picked diatom samples prepared for Si isotope analyses using an *Agillent 7500 Series* quadrupole ICPMS at GEOMAR in Kiel to check for potential remaining contamination by clays (Table 2). The reproducibility was better than 10% for Al/Si and better than 12% for Ti/Si ratio determination based on repeated sample measurements.

For Si isotope measurements, all samples were chromatographically purified following the method of Georg et al. (2006) as modified by de Souza et al. (2012a). Si isotope ratios were measured on a *NuPlasma HR* MC-ICPMS (Nu Instruments) at GEOMAR, which is equipped with an adjustable source-defining slit set to medium resolution to ensure separation of the ^{30}Si peak from molecular interferences. Measurements were carried out with a standard-sample bracketing method (Albarède et al., 2004). All solutions were measured at a Si concentration of 14–21 μmol/kg depending on the performance of the instrument and were introduced into the plasma via a Cetac Aridus II desolvator equipped with a PFA nebulizer at a 60 to 80 μL/min uptake rate. Si isotope compositions are reported in the $\delta^{30}Si$ notation of deviations of the measured $^{30}Si/^{28}Si$ from the international Si standard NBS28 in parts per thousand (‰):

$$\delta^{30}Si = \left[\frac{^{30}Si/^{28}Si_{sample}}{^{30}Si/^{28}Si_{standard}} - 1\right] * 1000$$

Repeated measurements of the reference materials IRMM018 and Big Batch gave average $\delta^{30}Si$ values of $-1.55 \pm 0.28‰$ ($2\sigma_{sd}$, $n = 38$) and $-10.80 \pm 0.22‰$ ($2\sigma_{sd}$, $n = 38$), respectively, which are in good agreement with values obtained by other laboratories (Reynolds et al., 2007).

Samples were measured three to five times during a daily session, which generally resulted in uncertainties between 0.07‰ and 0.40‰ ($2\sigma_{sd}$), with one sample having a $2\sigma_{sd}$ of 0.48‰ (Tables 1 and 2). Replicate measurements of in-house matrix standards for both seawater and diatom samples over a time period of one year gave a reproducibility of 0.25‰ ($2\sigma_{sd}$, $n = 12$ for a water sample and $n = 22$ for a sedimentary diatom sample, respectively), which corresponds to all error bars of the Si isotope compositions provided in the figures.

3. RESULTS

3.1. Water stations

3.1.1. Subsurface and bottom waters

The water column profiles (Fig. 3, Table 1) show a general increase in $Si(OH)_4$ concentrations with water depth. Only at St. 77 the highest concentration (40 µmol/kg) was found at 50 m depth and then decreased again to 30 µmol/kg near the bottom of the profile. Subsurface

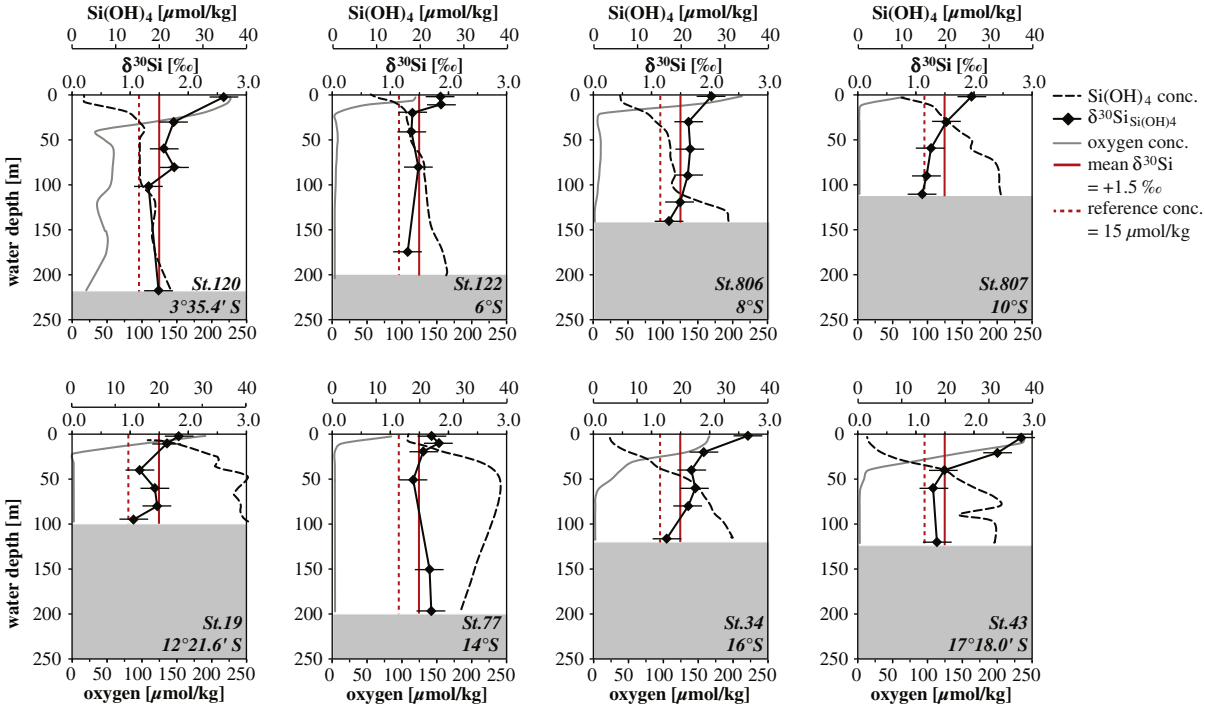

Fig. 3. Water column profiles for eight stations along the Ecuadorian and Peruvian shelf from north (top, left) to south (bottom, right) (see Fig. 1b). The grey shading indicates the bottom depth. For all stations the $\delta^{30}Si_{Si(OH)_4}$ (‰, black diamonds) and the $Si(OH)_4$ concentrations (µmol/kg, dashed black line) are shown. The grey solid line indicates the dissolved oxygen concentration (µmol/kg). The solid and dashed red lines mark the mean subsurface $\delta^{30}Si_{Si(OH)_4}$ of +1.5‰ (mean of the data for 50–150 m water depth of all 8 stations) and the reference $Si(OH)_4$ concentration of ~15 µmol/kg of the northernmost station, respectively. Error bars represent 0.25‰ $2\sigma_{sd}$ long-term reproducibility of repeated sample measurements.

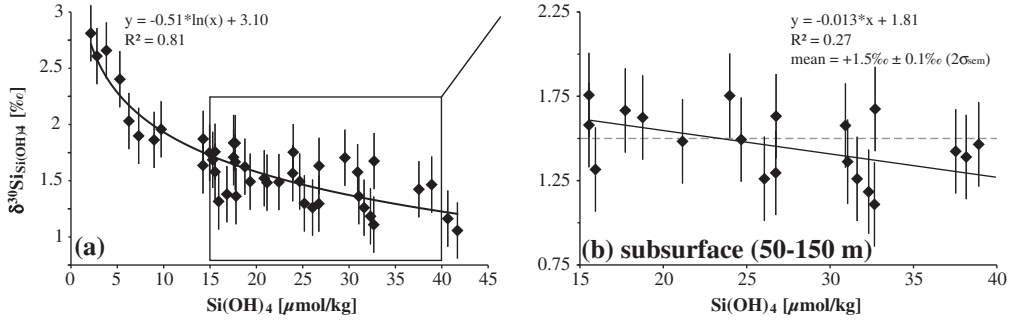

Fig. 4. Correlation between dissolved $\delta^{30}Si_{Si(OH)_4}$ (‰) and $Si(OH)_4$ concentrations (µmol/kg) for (a) all seawater samples, (b) subsurface samples between 50 and 150 m water depth, which are all characterised by $Si(OH)_4$ concentrations between 15 and 40 µmol/kg. The grey dashed line indicates the mean subsurface $\delta^{30}Si_{Si(OH)_4}$ of +1.5‰. Error bars represent 0.25‰ $2\sigma_{sd}$ long-term reproducibility of repeated sample measurements.

water $\delta^{30}Si_{Si(OH)_4}$ signatures and $Si(OH)_4$ concentrations show no distinct correlation (Fig. 4b). The subsurface waters flow southward along the shelf at 50–150 m water depth (Czeschel et al., 2011). In the northernmost St. 120, the concentration is influenced by the incoming EUC, which has a $Si(OH)_4$ concentration of 15 μmol/kg (red dashed line in Fig. 3). Towards the south the $Si(OH)_4$ concentration in this water depth range increases. The highest subsurface $Si(OH)_4$ concentrations are found at St. 19 and St. 77 between 12°S and 14°S (~40 μmol/kg). Further to the south concentrations decrease again (~30 μmol/kg). The patterns of the $\delta^{30}Si_{Si(OH)_4}$ profiles of all water column stations mirror those of the $Si(OH)_4$ concentrations in that the $\delta^{30}Si_{Si(OH)_4}$ values decrease with increasing water depth and $Si(OH)_4$ concentration. The mean $\delta^{30}Si_{Si(OH)_4}$ between 50 and 150 m water depth, which corresponds to the source depth of the upwelling waters, is $+1.5 \pm 0.1‰$ ($2\sigma_{sem}$, $n = 21$) (marked by the red solid line in Fig. 3). At most of the stations the deepest samples represent bottom waters (see Fig. 3, Table 1) and their $\delta^{30}Si_{Si(OH)_4}$ was also found to be near +1.5‰. Only at St. 807 and St. 19 between 10°S and 12°S the $\delta^{30}Si_{Si(OH)_4}$ of the bottom waters is somewhat lighter at values of +1.1‰.

3.1.2. Surface waters

In the surface waters the concentration of $Si(OH)_4$ varies widely with latitude and upwelling intensity. The highest concentrations of $Si(OH)_4$ (17.72 μmol/kg, Fig. 3, Table 1) are found close to the coast around 12° to 14°S, where the upwelling is very intense as evidenced by pronouncedly low SSTs (Fig. 2a). To the north and south of this area, the concentrations of $Si(OH)_4$ are lower, with minimum values reaching 2.14 μmol/kg. The surface waters show higher $\delta^{30}Si_{Si(OH)_4}$ values than the subsurface waters in all profiles, ranging from +1.7‰ to +2.8‰ (Fig. 3). The highest $\delta^{30}Si_{Si(OH)_4}$ values between +2.6‰ and +2.8‰ were found at the northernmost station (St. 120, 4°S) and at the stations south of 15°S (St. 34, St. 43). Low $\delta^{30}Si_{Si(OH)_4}$ values in surface waters ranging between +1.7‰ and +2.0‰ were found along the shelf at St. 122, 806, 807, 19 and St. 77 (between 6°S and 15°S), with the latter showing the minimum value. The $\delta^{30}Si_{Si(OH)_4}$ values of the surface waters show a clear negative correlation with $Si(OH)_4$ concentration (Fig. 4a, see Table 1).

3.2. Surface sediments

The highest $bSiO_2$ concentrations in the sediment, up to 21 wt%, are found close to the coast between 10° and 15°S (Fig. 5b). North and south of this area the fraction of $bSiO_2$ in the shelf sediments is much lower and reaches values as low as 0.24 wt% at 3°S. The $\delta^{30}Si_{bSiO_2}$ values range between −1.0‰ and +1.1‰, with the highest values found at 15°S (Fig. 5c, Table 2). Along the shelf between 5° and 10°S, where $bSiO_2$ concentrations are lower, the values range between +0.3‰ and +0.8‰. The lowest values of −1.0‰ and −0.4‰ are found at 17°S and 2°N, respectively. The $\delta^{30}Si_{diatom}$ values of the hand-picked diatoms are generally significantly higher than those of the $bSiO_2$ in the same samples with $\delta^{30}Si_{diatom}$ ranging between +0.6‰ and +2.0‰ (Fig. 5c, Table 2). Al/Si and Ti/Si ratios of hand-picked diatoms and $bSiO_2$-samples range from 1 to 235 mmol/mol and 31 to 160 μmol/mol, respectively (Fig. 6b, Table 2).

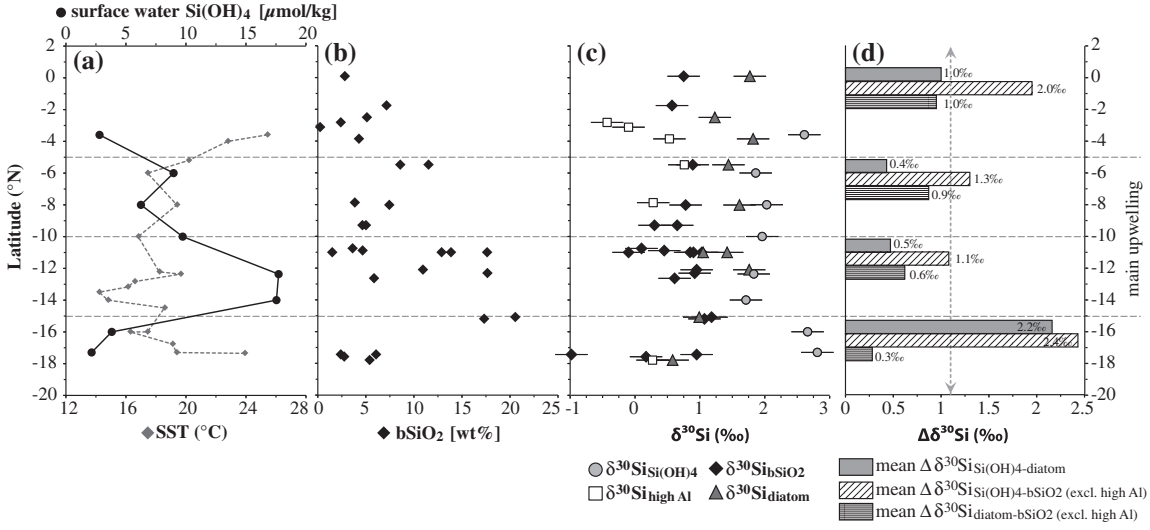

Fig. 5. Latitudinal distribution of (a) surface water $Si(OH)_4$ concentration (μmol/kg) and SST (°C), (b) surface sediment $bSiO_2$ concentration (wt%), (c) $\delta^{30}Si$ (‰) for surface waters (light grey dots), hand-picked diatoms (dark grey triangles), $bSiO_2$ (black diamonds) and $bSiO_2$ samples with high Al/Si ratios (white squares, see Fig. 6), (d) $\Delta\delta^{30}Si$ (‰) is the difference between surface water and sedimentary silicate phases (picked diatoms and $bSiO_2$ excluding the samples with high Al/Si ratios). Plotted are mean values for each latitudinal sector. The dotted vertical arrow indicates the theoretical $\Delta\delta^{30}Si$ of 1.1‰ between surface waters and picked diatoms/$bSiO_2$, assuming steady state. Error bars represent 0.25‰ $2\sigma_{sd}$ long-term reproducibility of repeated sample measurements. The horizontal grey dashed lines indicate the same latitudinal sectors as in Fig. 2.

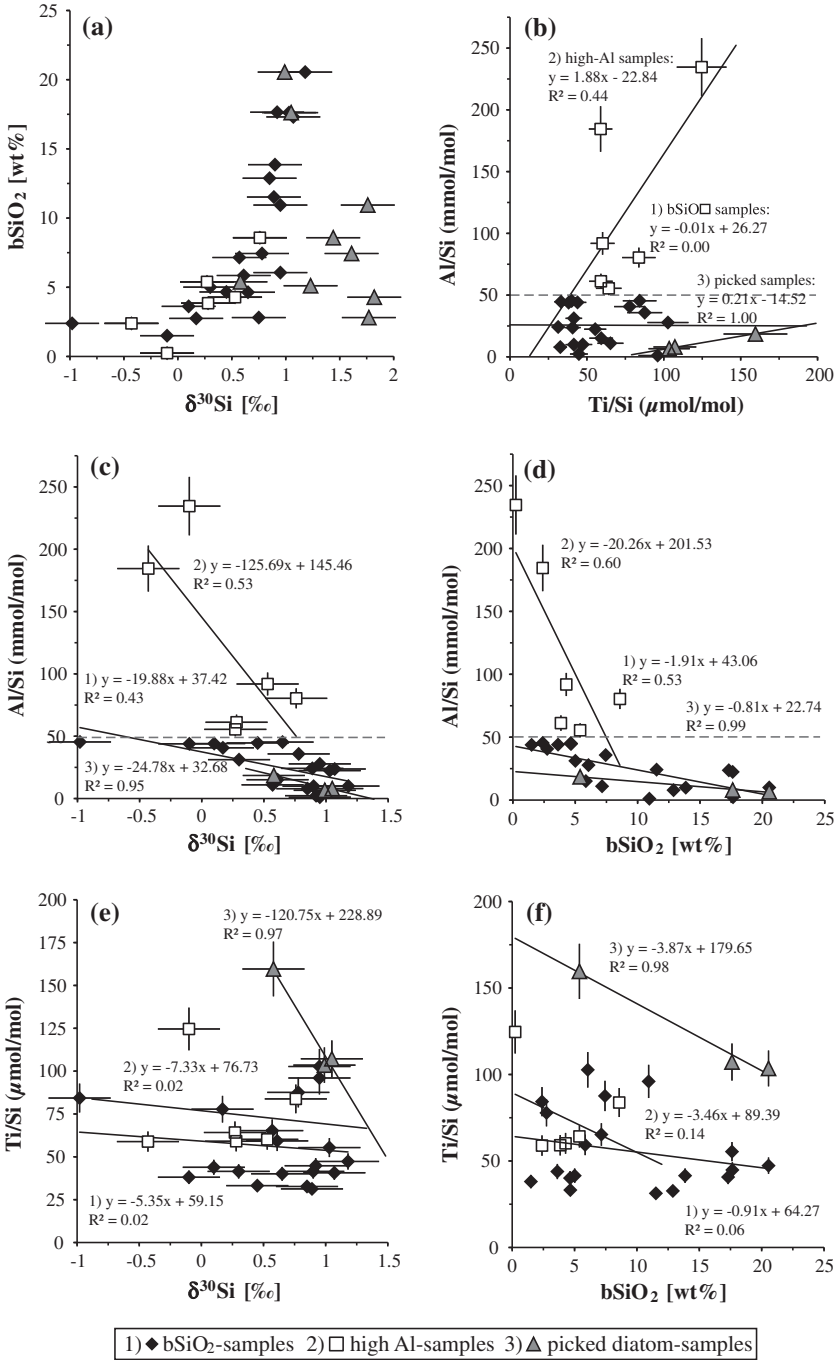

Fig. 6. Plots for surface sedimentary $bSiO_2$ (black diamonds) and picked diatom (grey triangles) samples for $bSiO_2$ concentration, $\delta^{30}Si$ data, Al/Si and Ti/Si ratios. The grey dashed line at Al/Si ratios of 50 mmol/mol indicates the threshold above which the samples are considered to be affected by lithogenic clay minerals (high-Al samples, white squares). Note that Al/Si and Ti/Si ratios were not measured for all samples (see Table 2).

4. DISCUSSION

4.1. Silicon isotope distribution in the water column

4.1.1. Subsurface and bottom waters

Upwelling along the Peruvian shelf is sourced from the southward flowing subsurface waters of the PCUC and the PCCC (Fig. 1), which mainly originate from the EUC and SSCC (Brink et al., 1983; Penven et al., 2005; Kessler, 2006). During January and February 2009, when the samples were taken, the PCUC was clearly detectable by ADCP along the shelf between 50 and 150 m water depth at 6°S, where station 122 is located. At 14°S (St. 77) the southward directed PCCC joined the PCUC and they were no longer distinguishable (Czeschel et al., 2011). Subsurface waters between 50 and 150 m, reflecting the main source for the

upwelling (Huyer et al., 1987; Karstensen and Ulloa, 2009; Czeschel et al., 2011), are characterized by a mean $\delta^{30}Si_{Si(OH)_4}$ signature of $+1.5‰ \pm 0.1‰$ ($2\sigma_{sem}$). The $Si(OH)_4$ concentration of the incoming subsurface waters at the northerly stations is around 15 μmol/kg (Fig. 3). The subsurface waters (characterised by $Si(OH)_4$ concentrations between 15 and 40 μmol/kg, Fig. 4b) display no significant correlation between the (southward increasing) $Si(OH)_4$ concentration and the $\delta^{30}Si_{Si(OH)_4}$, which shows that the subsurface water masses of the PCCC, the PCUC, and the northward flowing PCoastalC are not clearly distinguishable in their Si isotope composition. Previous studies found that subsurface water masses in the EEP have relatively homogenous $\delta^{30}Si_{Si(OH)_4}$ signatures around +1.5‰, but varying $Si(OH)_4$ concentrations (Beucher et al., 2008, 2011; de Souza et al., 2012b). Therefore, the significant increase in $Si(OH)_4$ concentrations within the subsurface waters from 15 to 40 μmol/kg along their southward flowpath, which is accompanied by essentially invariant $\delta^{30}Si_{Si(OH)_4}$ signatures most likely indicating lateral water mass mixing. However, there is also clear evidence for extensive remineralisation processes occurring both in the water column and from the shelf sediments (Franz et al., 2012). In upwelling areas like off Peru or California the preservation of $bSiO_2$ from blooming events is very high, as reflected by dissolution:production ratios around 0.1 (Nelson et al., 1981; Brzezinski et al., 2003), i.e. 90% of the produced $bSiO_2$ from the mixed layer is not dissolved and re-cycled but is exported below the mixed layer. In contrast, during non-blooming conditions the recycling is much stronger. Dissolution of $bSiO_2$ is expected to lead to lower $\delta^{30}Si_{Si(OH)_4}$ signatures in the water column, an effect that may be enhanced by the fractionation of Si isotopes during dissolution of $bSiO_2$ of −0.55‰ (Demarest et al., 2009). Analyses of shelf bottom waters showed very high concentrations of dissolved $Si(OH)_4$ which were most likely released from the sediments due to dissolution processes (Franz et al., 2012). However, it is only in two bottom water samples close to the sediment–water interface (St. 807, 19) where direct indications for an influence of dissolution on seawater $\delta^{30}Si_{Si(OH)_4}$ values are found ($\delta^{30}Si_{Si(OH)_4}$ shows a slight shift to values as low as +1.1‰, Fig. 3).

4.1.2. Surface waters

The surface waters along the Peruvian shelf can be separated into different latitudinal sectors (0–5°S, 5–10°S, 10–15°S, 15–20°S) according to their different physical (SST) and biological (chlorophyll *a* concentration) properties (Fig. 2). Due to variability in upwelling intensity, surface productivity is not homogenously distributed. The strongest upwelling occurs between 5°S and 15°S, which is also the area of the most intense OMZ. The highest chlorophyll *a* concentrations in that area are derived from diatom blooms (Bruland et al., 2005; Franz et al., 2012), which corroborates that primary productivity is driven by diatoms. Diatom growth is largely driven by the supply of $Si(OH)_4$ (Franz et al., 2012), which is strongest within the main upwelling region between 5°S and 15°S (Fig. 2c, 5a) and decreases towards the north (0°N to 5°S), the south (15°S to 20°S) and further offshore. $Si(OH)_4$ concentrations in surface waters of the coastal upwelling area off Peru are high where strong upwelling promotes continuous supply of deeper waters feeding the surface water pool. Conversely, they are lower in those areas where the delivery through upwelling is not as strong and primary productivity utilises the nutrients in the surface water more completely. The $\delta^{30}Si_{Si(OH)_4}$ difference between the subsurface source waters and the surface waters above, which directly reflects the utilisation of $Si(OH)_4$, amounts to only about 0.2–0.3‰ between 10°S and 15°S and around 0.5‰ between 5°S and 10°S (Fig. 3) within the main upwelling zone. Along the northern and southern areas of the shelf between 0°N and 5°S and south of 15°S, where upwelling is far less intense (areas of higher SSTs in Figs. 2a and 5a), the differences reach up to 1.1‰ and 1.3‰, respectively. The surface water $\delta^{30}Si_{Si(OH)_4}$ values thus directly reflect the availability of $Si(OH)_4$ in the euphotic zone (Fig. 2c, 5a and c): higher $Si(OH)_4$ concentrations in the surface water are associated with higher primary productivity (as supported by the surface water chlorophyll *a* concentration, Fig. 2b and c) (Bruland et al., 2005), but lower $\delta^{30}Si_{Si(OH)_4}$ values (Fig. 5a and c). Thus in the surface waters outside the upwelling region there is a higher degree of utilisation of $Si(OH)_4$ due to phytoplankton productivity, but at the same time $bSiO_2$ productivity is lower (Fig. 5a, c). The maximum difference between surface and subsurface Si isotope composition of 1.2‰ is even higher, and the $\delta^{30}Si_{Si(OH)_4}$ gradient sharper, than in areas of highly depleted surface $Si(OH)_4$ concentrations, such as the subtropical gyres (Reynolds et al., 2006). However, even within the main upwelling region, nearly continuous re-supply of $Si(OH)_4$ to the surface cannot prevent at least a slight Si isotope fractionation of the $Si(OH)_4$ in the surface waters.

4.1.3. Silicon isotope fractionation models

The Si isotope fractionation factor for the formation of diatom silica from seawater assessed by culture experiments is −1.1‰ in $\delta^{30}Si$ (De La Rocha et al., 1997). Two different models can approximate the evolution of the $\delta^{30}Si$ composition of surface waters during biologically induced fractionation from a reservoir with a given concentration and isotopic composition: a steady-state model (Fig. 7a), wherein a continuous supply and partial consumption of nutrients causes a dynamic equilibrium of the $Si(OH)_4$ content and the produced $bSiO_2$, and a Rayleigh-type model (Fig. 7b), in which after a single input no additional nutrients are newly supplied to the system (Mariotti et al., 1981; De La Rocha et al., 1997; Cardinal et al., 2005; Reynolds et al., 2006). The two models can be described by simple equations:

Steady-state system

$$\delta^{30}Si_{Si(OH)_4 obs} = \delta^{30}Si_{Si(OH)_4 source} - {}^{30}\varepsilon^{*}(1-f)$$

$$f = Si(OH)_{4_{obs}}/Si(OH)_{4_{source}}$$

$$\delta^{30}Si_{diatom} = \delta^{30}Si_{Si(OH)_4 obs} + {}^{30}\varepsilon$$

where $\delta^{30}Si_{Si(OH)_4 obs}$ is the Si isotope composition measured in the surface water after utilisation, $\delta^{30}Si_{Si(OH)_4 source}$ is the source Si isotope composition of the water, f is the depletion factor describing the fraction of the initial $Si(OH)_4$

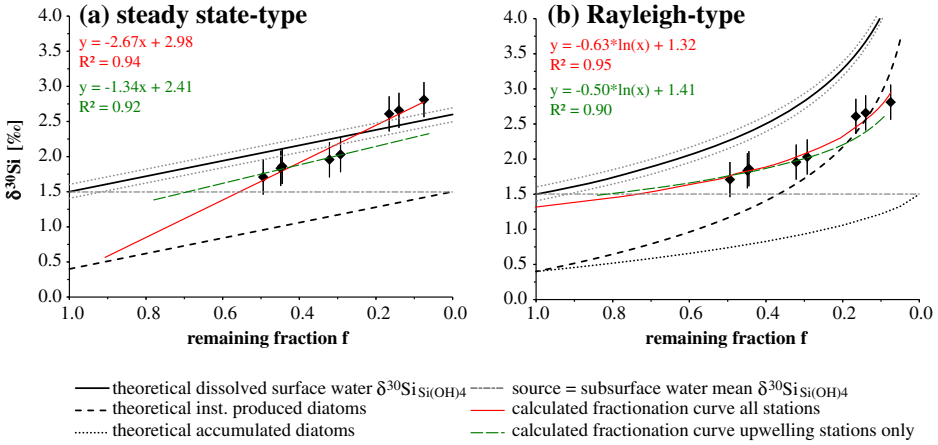

Fig. 7. $\delta^{30}Si_{Si(OH)_4}$ (‰) versus f (remaining $Si(OH)_4$ from the available pool) indicating the fractionation factor for (a) steady state-type and (b) Rayleigh-type conditions (using a logarithmic function). The solid black lines in the graphs indicate the fractionation curve of surface water $Si(OH)_4$ for a −1.1‰ fractionation, assuming an initial source value of +1.5‰ (dashed grey line, the dotted grey lines indicate the uncertainty of the source $\delta^{30}Si_{Si(OH)_4}$ value of +1.5‰ ± 0.1‰ ($2\sigma_{sem}$)), whereas the dashed black lines indicates the expected fractionation curve for the (instantaneously) produced diatoms as a result of a −1.1‰ fractionation, and the dotted black line indicates the accumulated diatoms under Rayleigh-type conditions. Calculated fractionation curves are given for all stations (red solid lines) and the upwelling-influenced stations only (5–15°S, dashed green lines). Error bars represent 0.25‰ $2\sigma_{sd}$ long-term reproducibility of repeated sample measurements. (For interpretation of the references to colour in this figure legend, the reader is referred to the web version of this article.)

concentration that remains, $^{30}\varepsilon$ is the fractionation factor associated with diatom uptake of $Si(OH)_4$ and $\delta^{30}Si_{diatom}$ is the Si isotope composition of the produced diatoms. Under assumed steady state conditions the supply of $Si(OH)_4$ equals the effective net $bSiO_2$ export (e.g. during one year) plus the residual $Si(OH)_4$ (e.g. Fripiat et al., 2011b).

Rayleigh-type system:

$$\delta^{30}Si_{Si(OH)_4obs} = \delta^{30}Si_{Si(OH)_4init} - {}^{30}\varepsilon * (\ln f)$$

$$\delta^{30}Si_{diatom\ inst} = \delta^{30}Si_{Si(OH)_4obs} + {}^{30}\varepsilon$$

$$\delta^{30}Si_{diatom\ acc} = \delta^{30}Si_{Si(OH)_4init} - {}^{30}\varepsilon * (f \ln f / 1 - f)$$

where $\delta^{30}Si_{Si(OH)_4init}$ is the Si isotope composition of $Si(OH)_4$ in the surface water before biological utilisation starts to fractionate the Si isotopes, $\delta^{30}Si_{diatom\ inst}$ is the Si isotope composition of the instantaneously produced diatoms at each time and $\delta^{30}Si_{diatom\ acc}$ is the Si isotope composition of the accumulated diatoms which integrate the fractionation over time. Both models assume a constant fractionation factor. The value of $^{30}\varepsilon$ is given by the slope of the linear regression between $\delta^{30}Si_{Si(OH)_4obs}$ and f for the steady-state model and between $\delta^{30}Si_{Si(OH)_4obs}$ and $\ln f$ for the Rayleigh-type system model (Fig. 7).

The mean $Si(OH)_4$ concentration for the depth between 50 and 150 m (or bottom water where the water depth is shallower), is employed as the initial concentration of the upwelling source waters at each station (Huyer et al., 1987; Karstensen and Ulloa, 2009) (Table 1). These waters show a relatively uniform $\delta^{30}Si$ of +1.5‰ ± 0.1‰ ($2\sigma_{sem}$, $n = 21$), which is consequently defined as the source water signature (Fig. 7). Both models were applied for surface waters only (shallowest samples at each station, usually between 2 and 4 m water depth, see Table 1) although utilisation might also occur below. However, given that Franz et al. (2012) have shown that the highest abundance of diatoms along the Peruvian shelf is primarily restricted to the upper 10 m (and less abundant up to 20 m water depth) of the water column our approach of defining the surface waters is justified. The fractionation factors $^{30}\varepsilon$ calculated for all 8 stations range between −2.7‰ (steady state) and −0.6‰ (Rayleigh) (Fig. 7), and thus deviate significantly from the experimentally determined $^{30}\varepsilon$ of −1.1‰ (De La Rocha et al., 1997). These discrepancies in the calculated fractionation factors are not surprising and arise from the fact that the estimation of the fractionation factor is easily biased by extensive mixing (Reynolds et al., 2006; Fripiat et al., 2011b). The calculated fractionation factor is very sensitive to the large contrast between the surface $\delta^{30}Si_{Si(OH)_4}$ values at stations influenced by stronger upwelling and those influenced by weaker upwelling. Calculating the fractionation factor for the upwelling-influenced stations only (between 5°S and 15°S) results in a fractionation factor for steady state-type conditions of −1.3‰ (Fig. 7a), which is indistinguishable from the experimentally derived $^{30}\varepsilon$ of −1.1‰ (De La Rocha et al., 1997). With the assumed source $\delta^{30}Si_{Si(OH)_4}$ signature of +1.5‰, and considering the error bars of the measurements, the data points only fit the theoretical surface water fractionation line (black solid line) of the steady state model (Fig. 7a), and not that the Rayleigh model (Fig. 7b). Here all data points lie below the theoretical curve. This is a reasonable result for the upwelling area, which, like most other areas of the ocean (De La Rocha et al., 2011), is not expected to be a Rayleigh-type system due to the continuous re-supply of upwelled nutrients. In the northern and southern sectors characterised by weaker upwelling, however, there is additional lateral transport of water masses with depleteded $Si(OH)_4$. Even though here, the surface water evolution follows a Rayleigh-like trend (away from the main upwelling, as indicated by the surface water fractionation curve in Fig. 7b) which is disrupted by more irregularly occurring upwelling events.

The calculated utilisation of available $Si(OH)_4$ in surface waters on the shelf ranges from about 51% in the main upwelling region to up to 93% further south (utilisation $[\%] = (1 - f) * 100$).

Usually, the models are used to estimate the fractionation factor $^{30}\varepsilon$ between the $Si(OH)_4$ and the $bSiO_2$ during diatom formation (e.g. Varela et al., 2004; De La Rocha et al., 2011; Fripiat et al., 2011b) or to validate the assumed initial source conditions (e.g. Reynolds et al., 2006; Cao et al., 2012). However, along the Peruvian shelf region the initial conditions are rather well constrained. The question is, which model can be applied in which region along the shelf, whether the fractionation conditions during $bSiO_2$ formation are reflected in the sediments and, reciprocally, whether they can be used to reconstruct past upwelling conditions.

4.2. Surface sediments

The distribution of $bSiO_2$ concentration in surface sediments agrees well with primary productivity in the surface waters in that the highest concentrations are found at those locations where the upwelling is most intense between 5°S and 15°S (and most pronounced between 10°S and 15°S) (Fig. 5a, b). This is also where the $\delta^{30}Si_{Si(OH)_4}$ of the surface water indicates the lowest fractionation with respect to the source signal (Fig. 5c). Correspondingly, diatoms deposited in the underlying surface sediments should also have the lowest $\delta^{30}Si$ values between 5°S and 15°S. In fact, however, along the entire shelf off Peru, the $\delta^{30}Si_{bSiO_2}$ values show no distinct variability (Fig. 5c). Overall, the highest $\delta^{30}Si_{bSiO_2}$ values are even found in the area of the strongest upwelling.

Calculation of the difference between the mean Si isotope signatures of surface waters and the $bSiO_2$ ($\Delta\delta^{30}Si_{Si(OH)_4\text{-}bSiO_2}$) in the different sectors along the shelf (Fig. 5d) indicates that the offset along the central shelf (5°S to 15°S) is around 1.1–1.3‰. In contrast, in the northern (0°N to 5°S) and southern (15°S to 20°S) sectors the offset is much larger at 2.0‰ and 2.4‰, respectively. Under assumed steady state conditions, the expected difference between seawater and sedimentary diatoms is 1.1‰ (De La Rocha et al., 1997). Along the central shelf region, where upwelling is strong, both sedimentary $\delta^{30}Si_{bSiO_2}$ and surface water $\delta^{30}Si_{Si(OH)_4}$ seem to support the assumption that $Si(OH)_4$ utilisation in this region can be best characterised by the steady state model. However, as shown by the fractionation models (Fig. 7) and the large offset between water and sediment, the areas north and south of the upwelling region do not seem to fit the steady state model assumptions (or the fractionation factor must be higher than −1.1‰).

In addition, along the whole shelf region some $bSiO_2$ samples display very light $\delta^{30}Si_{bSiO_2}$ values of up to −1.0‰ (Fig. 5c). Fig. 6a indicates that these light Si isotope signatures are mostly associated with samples having extremely low $bSiO_2$ concentrations, whereas samples having higher $bSiO_2$ concentrations also have higher $\delta^{30}Si_{bSiO_2}$ values. This is opposite to the expected trends in an upwelling area: high $bSiO_2$ concentrations are expected to prevail where the highest delivery of nutrients occurs and where correspondingly only weak Si isotope fractionation occurs (as shown by the surface waters). Instead, the measured $\delta^{30}Si_{bSiO_2}$ may not reflect diatoms only but may be due to the presence of silicates of other biogenic or lithogenic origin.

4.2.1. Possible clay contamination

The most obvious possibility for such other sources would be a contamination with clay minerals. Along the Peruvian shelf region, clay minerals are highly abundant in the sediments, with contributions of the <4 μm clay-size fraction of 40% to more than 60%, and originate both from riverine and aeolian input (Krissek et al., 1980; Scheidegger and Krissek, 1982). Clay minerals were found to have light $\delta^{30}Si$ values between −2.5‰ and 0‰ (Douthitt, 1982; Georg et al., 2009). Thus, if the cleaning process of the diatoms was not sufficiently rigorous, remaining and (partially) dissolved clay minerals in the sample solution would shift the measured $\delta^{30}Si_{bSiO_2}$ towards lower values (Ding et al., 1996; De La Rocha et al., 2000; Georg et al., 2009). In order to exclude the possibility of significant contributions from lithogenic clay mineral sources, Al/Si and Ti/Si ratios were thus measured for most of the dissolved $bSiO_2$ samples (Fig. 6, Table 2). The ratios in these samples are between 1 and 235 mmol/mol for Al/Si ratios and between 31 and 160 μmol/mol for Ti/Si ratios (Fig. 6b). Both elements are generally present as trace elements in diatom frustules (Ellwood and Hunter, 1999) but, more importantly, are major elements in clay minerals at much higher concentrations (Al/Si ratios in clays are ~1000 mmol/mol). It is very difficult to demonstrate complete removal of all clay minerals from the diatoms (Shemesh et al., 1988). The Al content of living planktonic diatoms is generally very low at Al/Si ratios between 0.1 and 10 mmol/mol (Lewin, 1961; Shemesh et al., 1988; van Bennekom et al., 1989, 1991; Dixit et al., 2001), whereas sedimentary diatoms were found to have Al/Si ratios of up to 1600 mmol/mol (van Bennekom et al., 1989; Dixit et al., 2001). The concentration of trace elements in the $bSiO_2$ depends on the concentration of the medium they grew from (Ellwood and Hunter, 1999), i.e. higher concentration in the water leads to higher concentration in the $bSiO_2$. Aluminium can be passively incorporated in $bSiO_2$ immediately after deposition due to the formation of authigenic aluminosilicate minerals on the $bSiO_2$-surface at the sediment–water interface (van Cappellen and Qiu, 1997; Dixit et al., 2001; Ragueneau et al., 2005). This leads to an enrichment of Al in the $bSiO_2$, such that the amount of Al in the $bSiO_2$ increases with exposure time to bottom waters (Koning et al., 2007), complicating the interpretation of trace element measurements. Nevertheless, typical Al/Si ratios of clean diatoms in sediments should be below 50 mmol/mol (Hurd, 1973; van Bennekom et al., 1988), which is one order of magnitude lower than corresponding Al/Si ratios in silicate minerals (Ragueneau et al., 2005).

Most of the checked $bSiO_2$ samples in this study had Al/Si ratios <50 mmol/mol but were usually much lower (Fig. 6b, Table 2). Only six samples had Al/Si ratios >50 mmol/mol (Fig. 6b, called 'high-Al samples'), which have relatively high Ti/Si ratios. These relatively high trace element concentrations occur mostly in samples having low

$bSiO_2$ concentrations, with more pronounced Al than Ti contents (Fig. 6d, e). These samples are potentially contaminated with clay mineral-derived silicate, and the respective samples and $\delta^{30}Si_{bSiO_2}$ values are excluded from the further interpretation.

There are several samples which were considered to be clean (Al/Si <50 mmol/mol) and which do not show elevated Ti/Si ratios, but still reveal very low $\delta^{30}Si_{bSiO_2}$ values up to −1.0‰ (Figs. 5d, 6c and e). These are mostly samples which coincide with low $bSiO_2$ concentrations (Fig. 6a, d and f). Consequently, the reason for these exceptionally low $\delta^{30}Si_{bSiO_2}$ values must be another contaminant biogenic silica source. For example, siliceous sponge spicules have very low $\delta^{30}Si$ values of about −3‰ (Douthitt, 1982; De La Rocha, 2003; Hendry et al., 2010). The fact that the lowest $\delta^{30}Si_{bSiO_2}$ values occur in those sediments containing the lowest amounts of $bSiO_2$ (Fig. 6a) supports this hypothesis: in samples with low diatom concentrations, any remaining spicule will have a much larger impact than in samples with higher diatom concentrations. A bias to more negative $\delta^{30}Si_{bSiO_2}$ ratios due to a contamination with non diatom $bSiO_2$ is thus a likely explanation.

4.2.2. Comparison with hand-picked diatoms

A separation of diatoms from other $bSiO_2$ materials is not possible with the applied heavy liquid separation method, and sponge spicules and diatoms do not show a difference in resistivity to dissolution processes during the preparation for Si isotope analyses. In order to avoid spicules in the dissolved samples, large diatoms (125–250 μm size fraction) were hand-picked from the same sediment samples. The two different size fractions represent two different diatom assemblages and upwelling seasons/conditions. The $bSiO_2$-fraction consists mostly of specimens of *Chaetoceros* (which makes up to 40% of all specimens), *Thalassionema nitzschioides, Actinoptychus spp.*, and other species (Abrantes et al., 2007) that are indicative of strong upwelling conditions and spring blooming events (Rojas de Mendiola, 1981; Schrader and Sorknes, 1991; Abrantes et al., 2007). The coarse fraction from which the large diatoms were picked mostly contained specimens of *Coscinodiscus*. These are large centric diatoms which are especially abundant in the northern part of the study area in more tropical-oceanic (low-nutrient) waters, or when upwelling is weaker during austral summer (De Vries and Schrader, 1981; Brodie and Kemp, 1994). Although the different size fractions consist of different diatom assemblages, a species-dependent effect on the fractionation factor between surface water and diatoms can be neglected (De La Rocha et al., 1997; Milligan et al., 2004; Alleman et al., 2005). The $\delta^{30}Si_{diatom}$ data obtained from the hand-picked diatoms are significantly different from $\delta^{30}Si_{bSiO_2}$ and show generally higher isotope values ranging from +0.6‰ to +2.0‰ (Fig. 5c, Table 2). The minimum values were found at the southernmost station, whereas the northernmost stations have the highest values. Trace element ratios of the picked diatoms could unfortunately only be measured on three specimens. These have low Al/Si ratios below 20 mmol/mol, but high Ti/Si ratios compared to most of the $bSiO_2$ samples, above 100 μmol/mol (Fig. 6b).

The difference between the mean $\delta^{30}Si_{diatom}$ and $\delta^{30}Si_{bSiO_2}$ ($\Delta\delta^{30}Si_{diatom\text{-}bSiO2}$, Fig. 5d) is lowest (and within uncertainty of the measurements) in the southernmost area of the shelf, whereas it increases towards the north, with maximum differences of up to 1.0‰. A reason for this might be the different growing seasons of the diatom assemblages. The hand-picked diatoms represent the diatom growth and surface $Si(OH)_4$ utilisation during weaker upwelling in austral summer, explaining the heavier Si isotopic composition. This is also the time period when the water samples were collected. It might therefore not be surprising that the hand-picked diatoms represent these surface waters, i.e. the season where the available pool of $Si(OH)_4$ is depleted.

The high $\delta^{30}Si_{diatom}$ in the north are somewhat surprising, because they are higher than the assumed source signal of +1.5‰, which is only possible when they represent late-growing diatoms whose source signal is influenced by a pre-fractionated surface water $Si(OH)_4$ pool. In the following, the fractionation models will be used to estimate the $Si(OH)_4$ utilisation from the Si isotope values of sedimentary $bSiO_2$ and picked diatoms at the time of their formation. These utilisations will be compared to the actual measured ones.

4.2.3. Calculation of utilisation from the sedimentary $\delta^{30}Si$

From the surface water data it can be concluded that the central shelf region (5°S to 15°S) can be characterised by the steady state model. Therefore, the $bSiO_2$ and the picked diatoms from the underlying sediments can be directly used to reconstruct the Si isotope composition of the surface water at the time of their formation and the utilisation of available $Si(OH)_4$ at that time (Fig. 8a). The canonical fractionation factor $^{30}\varepsilon$ between the seawater and the diatoms is −1.1‰ (De La Rocha et al., 1997). By adding this value to the mean measured $\delta^{30}Si_{bSiO_2}$ and $\delta^{30}Si_{diatom}$ in that area of +0.7‰ and +1.3 to +1.5‰, respectively, the calculated theoretical surface water $\delta^{30}Si_{Si(OH)_4}$ values are +1.8‰ and +2.4 to +2.6‰. These values correspond to $Si(OH)_4$ utilisation of 25% and 90% (Fig. 8a) for $bSiO_2$ and picked diatoms respectively, considering the core top sediment isotope values from the main upwelling region. From the surface waters, the measured utilisation in that area ranges between 50% and 70%. The $bSiO_2$ samples thus underestimate this utilisation during summer upwelling conditions, which might be due to the fact that they grow earlier in the season when upwelling and nutrient supply is stronger. In contrast, the main picked diatom species, *Coscinodiscus*, grows later during austral summer and the calculated utilisation is close to the measured value.

Along the northern shelf region the surface water data have shown that the steady state model does not represent the data fully. We assume that the diatoms in that region are rather formed under more Rayleigh-type conditions (Fig. 8b). The diatoms, especially *Coscinodiscus*, represent here blooming events (Bruland et al., 2005) (i.e. they represent $\delta^{30}Si_{diatom\ inst}$ in the model). Therefore, the fractionation factor of −1.1‰ (or −0.6‰ calculated from all surface stations, see Fig. 7b) to calculate the surface water from which they were formed can also be used here. The

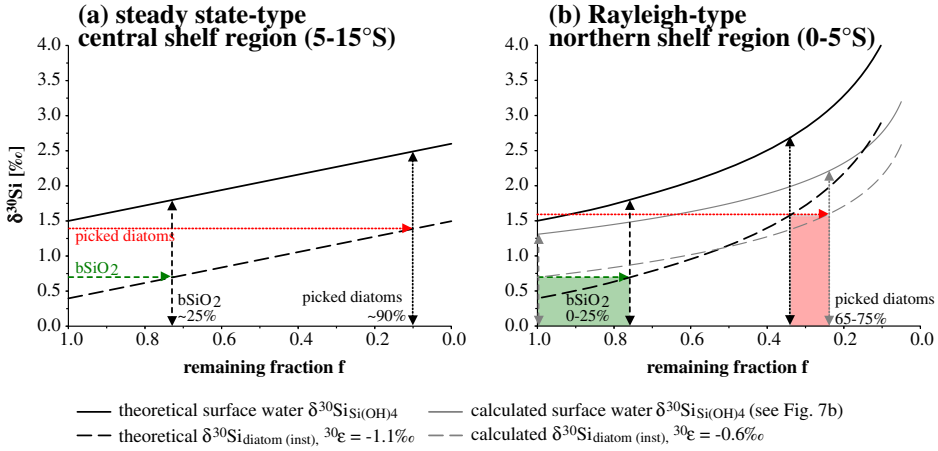

Fig. 8. Remaining fraction of $Si(OH)_4$ versus $\delta^{30}Si$ for $bSiO_2$ and picked diatom samples (‰) under (a) steady state conditions (characterising the samples within the upwelling region between 5 and 15°S) and (b) Rayleigh-type conditions (for the samples north of 5°S). The black solid and dashed curves indicate the fractionation behaviour for surface water and inst. Produced diatoms for a theoretical fractionation of −1.1‰, whereas the grey solid and dashed curves indicate the fractionation curves with a −0.6‰ fractionation calculated for Rayleigh-type conditions (see Fig. 7b). The horizontal arrows indicate the mean measured $\delta^{30}Si$ values for $bSiO_2$ (dashed, green) and picked diatom (dotted, red) samples, respectively, and the vertical arrows (black for the theoretical and grey for the calculated fractionation factor) indicate the resulting surface water $\delta^{30}Si_{Si(OH)_4}$ and $Si(OH)_4$ utilisation at the time of their formation. (For interpretation of the references to colour in this figure legend, the reader is referred to the web version of this article.)

mean $\delta^{30}Si_{diatom}$ value of +1.6‰ for picked diatoms corresponds to surface water values of up to +2.7‰ and surface water $Si(OH)_4$ utilisation of up to 75% (Fig. 8b). The measured utilisation in that area is of the same order, ca. 80%. In contrast, the $bSiO_2$ samples, with a mean $\delta^{30}Si_{bSiO_2}$ of +0.7‰, correspond to surface water $\delta^{30}Si_{Si(OH)_4}$ values of up to +1.8‰ and a $Si(OH)_4$ utilisation at the time of their formation of maximum only 40%. This is a very low value, comparable to those measured in the main upwelling region, even though the northerly region does not generally experience such conditions of strong upwelling and nutrient supply (Karstensen and Ulloa, 2009). This is the area of the lowest $bSiO_2$ concentrations in the sediment (Fig. 5b), and most likely the light $\delta^{30}Si_{bSiO_2}$ values are affected by a contaminating biogenic silica source with a lighter Si isotope signature.

Another interesting feature are the low $\delta^{30}Si$ values in both $bSiO_2$ and in the picked diatoms south of 15°S, which, except for one $bSiO_2$ sample, do not differ significantly from a value of about +0.6‰ to +0.7‰, excluding the sample with the lowest $\delta^{30}Si_{bSiO_2}$ of −1.0‰. In contrast, the surface waters in that area have high $\delta^{30}Si_{Si(OH)_4}$ values of about +2.7‰. The offset between both $bSiO_2$ and picked diatoms to the surface water is almost identical at around 2.3‰ (Fig. 5d). The most likely explanation for this contradictory picture is a southward transport of the diatoms within the subsurface currents. The diatoms have almost the same $\delta^{30}Si$ signatures as those in the main upwelling region (Fig. 5c). Due to the much lower upwelling conditions in the southern sector the productivity of diatoms in the surface water is much lower than further to the north (Fig. 2). Here, the shelf is much narrower, the supply of nutrients is weaker and the relative amount of diatoms on the total primary productivity is lower (Bruland et al., 2005; DiTullio et al., 2005). Therefore, it is likely that the majority of the diatoms were not formed in the surface waters south of 15°S, which have much higher $\delta^{30}Si_{Si(OH)_4}$ values, but originate from the more northerly surface waters from within the main upwelling region.

Overall, the $\delta^{30}Si_{diatom}$ signatures of the hand picked diatoms seem to preserve the utilisation signal much better and more reliably than the $\delta^{30}Si_{bSiO_2}$ values. Within the northern and central shelf sectors, the $\delta^{30}Si_{diatom}$ data show a similar distribution pattern to the $\delta^{30}Si_{Si(OH)_4}$ in the surface waters. They are low in the main upwelling region, and show much higher values along the northern part of the shelf between 5°S and 10°S. Although the actual values indicate a transfer of the surface water signal into the sediment, the picked diatoms from the surface sediments integrate the surface water signal over the late austral summer season of many years. Other factors such as (partial) dissolution would leave diatoms with a higher than initial $\delta^{30}Si$ signature. Ignoring this fractionation effect may result in an overestimation of the level of past $Si(OH)_4$ utilisation in surface waters and an underestimating of the calculated fractionation factor between seawater and diatoms. Finally, fundamentally different conditions during single years (e.g. El Nino events) are very likely to influence the deposited signature, which has to be taken into account for interpretations of past upwelling conditions. For example, a change in the source signal and a higher fractionation of $Si(OH)_4$ in the surface water during El Nino conditions due to diminished upwelling (Feldman et al., 1984; Fiedler, 2002) will most likely influence the signal preserved in the sediments.

The general assumption for all paleo-studies using Si isotopes as a proxy for $Si(OH)_4$ utilisation is that the major fraction of the $bSiO_2$ in the sediment consists of diatoms (De La Rocha et al., 1998; Brzezinski et al., 2002; Beucher et al., 2007; Reynolds et al., 2008). This is probably justified for studies of the Southern Ocean or the subpolar North

Pacific where $bSiO_2$ concentrations are usually higher than 10–20 wt%. However, the surface sediment distribution of $bSiO_2$ off Peru today (Fig. 5b) shows strong latitudinal gradients between high and low silica concentrations due to differences in upwelling intensity and nutrient supply. In the past, during times of overall low upwelling, the concentration of $bSiO_2$ might have also been low in areas where it is high today, e.g. in the Subantarctic Zone (Brzezinski et al., 2002; Bradtmiller et al., 2009). In this case, a significant influence of non-diatom $bSiO_2$ cannot be excluded, unless all samples are hand-picked to avoid contamination.

5. CONCLUSIONS

This study investigates the factors controlling the silicon isotope composition of dissolved silicic acid $\delta^{30}Si_{Si(OH)_4}$ in the water column and of the diatoms that grew in the surface waters ($\delta^{30}Si_{bSiO_2}$, $\delta^{30}Si_{diatom}$) of the Peruvian upwelling area.

Subsurface waters feeding the coastal upwelling off Peru display a mean $\delta^{30}Si_{Si(OH)_4}$ signature of $+1.5‰ \pm 0.1‰$ ($2\sigma_{sem}$) all along the Peruvian shelf, whereas the $Si(OH)_4$ concentration increases with latitude towards the south as a function of water mass mixing and remineralisation of $bSiO_2$ in the water column and in the sediments, as indicated by significant increases in $Si(OH)_4$ concentrations in the bottom waters above the shelf. The $\delta^{30}Si_{Si(OH)_4}$ distribution in the surface waters along the Peruvian shelf is mainly controlled by upwelling intensity. In the area of the strongest upwelling and re-supply of $Si(OH)_4$, where the degree of utilisation of $Si(OH)_4$ is overall low (about 50%), the difference between surface water $\delta^{30}Si_{Si(OH)_4}$ and the subsurface source waters caused by silicate utilisation amounts to only 0.2–0.3‰. Higher degrees of $Si(OH)_4$ utilisation (up to 93%) in surface waters outside the main upwelling area result in higher $\delta^{30}Si_{Si(OH)_4}$ values of up to 2.8‰, corresponding to a difference of up to 1.3‰ from the source water.

The calculation of the fractionation factor $^{30}\varepsilon$ based on our surface water $\delta^{30}Si_{Si(OH)_4}$ data gives values between −0.5‰ and −2.7‰ for Rayleigh-type and steady-state system conditions, respectively. This is a large deviation from the experimentally derived value of −1.1‰, which is caused by the strong influence of water mass mixing in this highly dynamic environment. However, $\delta^{30}Si_{Si(OH)_4}$ values in the main upwelling region reveal a fractionation factor of −1.3‰ for steady state conditions. Comparison of $\delta^{30}Si_{diatom}$ compositions obtained from hand-picked diatoms from the underlying sediments, which range from +0.6‰ to +2.0‰, shows the same overall distribution as that of $\delta^{30}Si_{Si(OH)_4}$. The biogenic silicate of these diatoms exhibits lower $\delta^{30}Si_{diatom}$ values in the main upwelling region, where productivity is highest. Along the northern shelf between 0 and 5°S, where upwelling and productivity are lower, the $Si(OH)_4$ utilisation and $\delta^{30}Si_{diatom}$ values are significantly higher.

A comparison between $\delta^{30}Si_{bSiO_2}$ signatures obtained from bulk $bSiO_2$ in the sediment, which was extracted applying commonly used methods, and $\delta^{30}Si_{diatom}$ from hand-picked diatoms indicates that in samples with low $bSiO_2$ concentrations a contamination with isotopically lighter biogenic siliceous material, such as sponge spicules or radiolarians, occurs. This observation has important implications for the general interpretation of paleo-$\delta^{30}Si$ records at locations with low $bSiO_2$ content and suggests that for sediments containing such low amounts of $bSiO_2$ significant biases of the $\delta^{30}Si$ records can only be excluded if it can be demonstrated that a pure diatom fraction was extracted.

ACKNOWLEDGMENTS

This work is a contribution of the Sonderforschungsbereich 754 "Climate – Biogeochemistry Interactions in the Tropical Ocean" (www.sfb754.de), which is supported by the Deutsche Forschungsgemeinschaft. Special thank goes to the crew of the RV Meteor. Many thanks also go to Birgit Glückselig, Ulrike Böttjer, and Rainer Gersonde from AWI, Bremerhaven, who helped to establish the diatom separation methods, and to Ed Hathorne for the elemental analyses on the Quadrupole ICP-MS. Analyses and visualisations of the satellite data used in this study were produced with the Giovanni online data system, developed and maintained by the NASA GES DISC.

REFERENCES

Abrantes F. F., Lopes C., Mix A. C. and Pisias N. G. (2007) Diatoms in Southeast Pacific surface sediments reflect environmental properties. *Quatern. Sci. Rev.* **26**(1–2), 155–169. http://dx.doi.org/10.1016/j.quascirev.2006.02.022.

Albarède F., Telouk P., Blichert-Toft J., Boyet M., Agranier A. and Nelson B. K. (2004) Precise and accurate isotopic measurements using multiple-collector ICPMS. *Geochim. Cosmochim. Acta* **68**(12), 2725–2744. http://dx.doi.org/10.1016/j.gca.2003.11.024.

Alleman L. Y., Cardinal D., Cocquyt C., Plisnier P.-D., Descy J.-P., Kimirei I. and Sinyinza D., et al. (2005) Silicon isotopic fractionation in Lake Tanganyika and its main tributaries. *J. Great Lakes Res.* **31**(4), 509–519.

Ayón P., Criales-Hernandez M. I., Schwamborn R. and Hirche H.-J. (2008) Zooplankton research off Peru: a review. *Prog. Oceanogr.* **79**(2–4), 238–255. http://dx.doi.org/10.1016/j.pocean.2008.10.020.

Berger W. H., Smetacek V. S. and Wefer G. (1989) *Productivity of the Ocean: Present and Past*. John Wiley & Sons, Berlin (Life Sci., p. 471).

Beucher C. P., Brzezinski M. A. and Crosta X. (2007) Silicic acid dynamics in the glacial sub-Antarctic: implications for the silicic acid leakage hypothesis. *Global Biogeochem. Cycles* **21**(GB3015). http://dx.doi.org/10.1029/2006GB002746.

Beucher C. P., Brzezinski M. A. and Jones J. L. (2008) Sources and biological fractionation of Silicon isotopes in the Eastern Equatorial Pacific. *Geochim. Cosmochim. Acta* **72**(13), 3063–3073. http://dx.doi.org/10.1016/j.gca.2008.04.021.

Beucher C. P., Brzezinski M. A. and Jones J. L. (2011) Mechanisms controlling silicon isotope distribution in the Eastern Equatorial Pacific. *Geochim. Cosmochim. Acta* **75**, 4286–4294. http://dx.doi.org/10.1016/j.gca.2011.05.024.

Bradtmiller L. I., Anderson R. F., Fleisher M. Q. and Burckle L. H. (2009) Comparing glacial and Holocene opal fluxes in the Pacific sector of the Southern Ocean. *Paleoceanography* **24**(PA2214). http://dx.doi.org/10.1029/2008PA001693.

Brink K. H., Halpern D., Huyer A. and Smith R. L. (1983) The physical environment of the Peruvian upwelling system. *Prog.*

Oceanogr. **12**(3), 285–305. http://dx.doi.org/10.1016/0079-6611(83)90011-3.

Brodie I. and Kemp A. E. S. (1994) Variation in biogenic and detrital fluxes and formation of laminae in late quaternary sediments from the Peruvian coastal upwelling zone. *Mar. Geol.* **116**, 385–398.

Bruland K. W., Rue E. L., Smith G. J. and DiTullio G. R. (2005) Iron, macronutrients and diatom blooms in the Peru upwelling regime: brown and blue waters of Peru. *Mar. Chem.* **93**(2–4), 81–103. http://dx.doi.org/10.1016/j.marchem.2004.06.011.

Brzezinski M. A., Pride C. J., Franck V. M., Sigman D. M., Sarmiento J. L., Matsumoto K. and Gruber N., et al. (2002) A switch from $Si(OH)_4$ to NO_3^- depletion in the glacial Southern Ocean. *Geophys. Res. Lett.* **29**(12). http://dx.doi.org/10.1029/2001GL014349.

Brzezinski M. A., Jones J. L., Bidle K. D. and Azam F. (2003) The balance between silica production and silica dissolution in the sea: insights from Monterey Bay, California, applied to the global data set. *Limnol. Oceanogr.* **48**(5), 1846–1854.

Cao Z., Frank M., Dai M., Grasse P. and Ehlert C. (2012) Silicon isotope constraints on sources and utilisation of silicic acid in the northern South China Sea. *Geochim. Cosmochim. Acta* **97**, 88–104. http://dx.doi.org/10.1016/j.gca.2012.08.039.

Cardinal D., Alleman L. Y., Dehairs F., Savoye N., Trull T. W. and André L. (2005) Relevance of silicon isotopes to Si-nutrient utilization and Si-source assessment in Antarctic waters. *Global Biogeochem. Cycles* **19**(GB2007). http://dx.doi.org/10.1029/2004GB002364.

Chavez F. P. (1995) A comparison of ship and satellite chlorophyll from California and Peru. *J. Geophys. Res.* **100**, 855–862.

Codispoti L. A., Brandes J. A., Christensen J. P., Devol A. H., Naqvi S. W. A., Paerl H. W. and Yoshinari T. (2001) The oceanic fixed nitrogen and nitrous oxide budgets: moving targets as we enter the anthropocene? *Sci. Mar.* **65**, 85–105.

Czeschel R., Stramma L., Schwarzkopf F. U., Giese B. S., Funk A. and Karstensen J. (2011) Middepth circulation of the eastern tropical South Pacific and its link to the oxygen minimum zone. *J. Geophys. Res.* **116**(C01015). http://dx.doi.org/10.1029/2010JC006565.

De La Rocha C. L. (2003) Silicon isotope fractionation by marine sponges and the reconstruction of the silicon isotope composition of ancient deep water. *Geology* **31**, 423–426. http://dx.doi.org/10.1130/0091-7613(2003) 031 < 0423.

De La Rocha C. L., Brzezinski M. A. and De Niro M. J. (1997) Fractionation of silicon isotopes by marine diatoms during biogenic silica formation. *Geochim. Cosmochim. Acta* **61**(23), 5051–5056. http://dx.doi.org/10.1016/S0016-7037(97)00300-1.

De La Rocha C. L., Brzezinski M. A., De Niro M. J. and Shemesh A. (1998) Silicon–isotope composition of diatoms as an indicator of past oceanic change. *Nature* **395**, 680–683.

De La Rocha C. L., Brzezinski M. A. and De Niro M. J. (2000) A first look at the distribution of the stable isotopes of silicon in natural waters. *Geochim. Cosmochim. Acta* **64**(14), 2467–2477. http://dx.doi.org/10.1016/S0016-7037(00)00373-2.

De La Rocha C. L., Bescont P., Croguennoc A. and Ponzevera E. (2011) The silicon isotopic composition of surface waters in the Atlantic and Indian sectors of the Southern Ocean. *Geochim. Cosmochim. Acta* **75**(18), 5283–5295. http://dx.doi.org/10.1016/j.gca.2011.06.028.

De Souza G. F., Reynolds B. C., Rickli J., Frank M., Saito M. A., Gerringa L. J. A. and Bourdon B. (2012a) Southern Ocean control of silicon stable isotope distribution in the deep Atlantic Ocean. *Global Biogeochem. Cycles* **26**(GB2035). http://dx.doi.org/10.1029/2011GB004141.

De Souza G. F., Reynolds B. C., Johnson G. C., Bullister J. L. and Bourdon B. (2012b) Silicon stable isotope distribution traces Southern Ocean export of Si to the eastern South Pacific thermocline. *Biogeosci. Discuss.* **9**(6), 6409–6443. http://dx.doi.org/10.5194/bgd-9-6409-2012.

De Vries T. J. and Schrader H. (1981) Variations of upwelling/oceanic conditions during the latest Pleistocene through Holocene off the central Peruvian coast: a diatom record. *Mar. Micropaleontol.* **6**, 157–167.

Demarest M. S., Brzezinski M. A. and Beucher C. P. (2009) Fractionation of silicon isotopes during biogenic silica dissolution. *Geochim. Cosmochim. Acta* **73**(19), 5572–5583. http://dx.doi.org/10.1016/j.gca.2009.06.019.

DeMaster D. J. (1981) The supply and accumulation of silica in the marine environment. *Geochim. Cosmochim. Acta* **45**(10), 1715–1732. http://dx.doi.org/10.1016/0016-7037(81)90006-5.

Ding T. P., Jiang S., Wan D., Li Y., Li J., Song H. and Liu Z., et al. (1996) *Silicon Isotope Geochemistry*. Geological Publishing House, Beijing, China, p. 125.

DiTullio G. R., Geesey M. E., Maucher J. M., Alm M. B., Riseman S. F. and Bruland K. W. (2005) Influence of iron on algal community composition and physiological status in the Peru upwelling system. *Limnol. Oceanogr.* **50**(6), 1887–1907.

Dixit S., van Cappellen P. and van Bennekom A. J. (2001) Processes controlling solubility of biogenic silica and pore water build-up of silicic acid in marine sediments. *Mar. Chem.* **73**, 333–352.

Douthitt C. B. (1982) The geochemistry of the stable isotopes of silicon. *Geochim. Cosmochim. Acta* **46**(8), 1449–1458. http://dx.doi.org/10.1016/0016-7037(82)90278-2.

Dugdale R. C., Wilkerson F. P. and Minas H. J. (1995) The role of a silicate pump in driving new production. *Deep Sea Res.* **42**(5), 697–719. http://dx.doi.org/10.1016/0967-0637(95)00015-X.

Ellwood M. J. and Hunter K. A. (1999) Determination of the Zn/Si ratio in diatom opal: a method for the separation, cleaning and dissolution of diatoms. *Mar. Chem.* **66**(3–4), 149–160. http://dx.doi.org/10.1016/S0304-4203(99)00037-7.

Estrada M. and Blasco D. (1985) Phytoplankton assemblages in coastal upwelling areas. In *Simposio Internacional Sobre Las Areas de Afloramiento Mas Importantes del Oeste Africano (Cabo Blanco y Benguela)* (eds. C. Bas, R. Margalef and P. Rubies). Instituto de Investigaciones Pesqueras, Barcelona, pp. 379–402.

Feldman G., Clark D. and Halpern D. (1984) Satellite color observations of phytoplankton distribution in the Eastern Equatorial Pacific during the 1982–1983 El Nino. *Science* **226**, 1069–1071.

Fiedler P. C. (2002) Environmental change in the Eastern tropical Pacific Ocean: review of ENSO and decadal variability. *Mar. Ecol. Prog. Ser.* **224**, 265–283.

Franz J., Krahmann G., Lavik G., Grasse P., Dittmar T. and Riebesell U. (2012) Dynamics and stoichiometry of nutrients and phytoplankton in waters influenced by the oxygen minimum zone in the eastern tropical Pacific. *Deep Sea Res.* **62**, 20–31. http://dx.doi.org/10.1016/j.dsr.2011.12.004.

Fripiat F., Cavagna A.-J., Dehairs F., Speich S., André L. and Cardinal D. (2011a) Silicon pool dynamics and biogenic silica export in the Southern Ocean inferred from Si-isotopes. *Ocean Sci.* **7**(5), 533–547. http://dx.doi.org/10.5194/os-7-533-2011.

Fripiat F., Cavagna A.-J., Savoye N., Dehairs F., André L. and Cardinal D. (2011b) Isotopic constraints on the Si-biogeochemical cycle of the Antarctic Zone in the Kerguelen area (KEOPS). *Mar. Chem.* **123**(1–4), 11–22. http://dx.doi.org/10.1016/j.marchem.2010.08.005.

Fuenzalida R., Schneider W., Garcés-Vargas J., Bravo L. and Lange C. B. (2009) Vertical and horizontal extension of the oxygen minimum zone in the eastern South Pacific Ocean. *Deep*

Sea Res. **56**(16), 1027–1038. http://dx.doi.org/10.1016/j.dsr2.2008.11.001.

Georg R. B., Reynolds B. C., Frank M. and Halliday A. N. (2006) New sample preparation techniques for the determination of Si isotopic compositions using MC-ICPMS. *Chem. Geol.* **235**(1–2), 95–104. http://dx.doi.org/10.1016/j.chemgeo.2006.06.006.

Georg R. B., Zhu C., Reynolds B. C. and Halliday A. N. (2009) Stable silicon isotopes of groundwater, feldspars, and clay coatings in the Navajo Sandstone aquifer, Black Mesa, Arizona, USA. *Geochim. Cosmochim. Acta* **73**(8), 2229–2241. http://dx.doi.org/10.1016/j.gca.2009.02.005.

Gunther E. R. (1936) A report on oceanographic investigations in the Peru Coastal Current. *Disc. Rep.* **13**, 107–276.

Hansen H. P. and Koroleff F. (1999) Determination of nutrients. In *Methods of Seawater Analysis* (eds. K. Grasshoff, K. Kremling and M. Erhardt), 3rd ed. Wiley VHC, pp. 159–228.

Hendry K. R., Georg R. B., Rickaby R. E. M., Robinson L. F. and Halliday A. N. (2010) Deep ocean nutrients during the Last Glacial Maximum deduced from sponge silicon isotopic compositions. *Earth Planet. Sci. Lett.* **292**(3–4), 290–300. http://dx.doi.org/10.1016/j.epsl.2010.02.005.

Hurd D. C. (1973) Interactions of biogenic opal, sediment and seawater in the Central Equatorial Pacific. *Geochim. Cosmochim. Acta* **37**(10), 2257–2282. http://dx.doi.org/10.1016/0016-7037(73)90103-8.

Huyer A., Smith R. L. and Paluszkiewicz T. (1987) Coastal Upwelling off Peru During Normal and El Niño Times, 1981–1984. *J. Geophys. Res.* **92**(C13), 14297–14307. http://dx.doi.org/10.1029/JC092iC13p14297.

Karl D. M. and Tien G. (1992) Magic: a sensitive and precise method for measuring dissolved phosphorus in aquatic environments. *Limnol. Oceanogr.* **37**(1), 105–116.

Karstensen J. and Ulloa O. (2009) The Peru-Chile current system. In *Ocean Currents: A Derivative of the Encyclopedia of Ocean Sciences* (eds. J. H. Steele, S. A. Thorpe and K. K. Turekian). (2nd edition). pp. 85–92.

Karstensen J., Stramma L. and Visbeck M. (2008) Oxygen minimum zones in the eastern tropical Atlantic and Pacific oceans. *Prog. Oceanogr.* **77**(4), 331–350. http://dx.doi.org/10.1016/j.pocean.2007.05.009.

Kessler W. S. (2006) The circulation of the eastern tropical Pacific: a review. *Prog. Oceanogr.* **69**(2–4), 181–217. http://dx.doi.org/10.1016/j.pocean.2006.03.009.

Koning E., Gehlen M., Flank A.-M., Calas G. and Epping E. (2007) Rapid post-mortem incorporation of aluminum in diatom frustules: evidence from chemical and structural analyses. *Mar. Chem.* **106**(1–2), 208–222. http://dx.doi.org/10.1016/j.marchem.2006.06.009.

Krissek L. A., Scheidegger K. F. and Kulm L. D. (1980) Surface sediments of the Peru–Chile continental margin and the Nazca plate. *Geol. Soc. Am. Bull.* **91**(6), 321–331. http://dx.doi.org/10.1130/0016-7606(1980) 91 < 321.

Lam P., Lavik G., Jensen M. M., Van de Vossenberg J., Schmid M., Woebken D. and Amann R., et al. (2009) Revising the nitrogen cycle in the Peruvian oxygen minimum zone. *Proc. Natl. Acad. Sci.* **106**(12), 4752–4757.

Lewin J. C. (1961) The dissolution of silica from diatom walls. *Geochim. Cosmochim. Acta* **21**(104), 182–198.

Lukas R. (1986) The termination of the Equatorial Undercurrent in the eastern Pacific. *Prog. Oceanogr.* **16**(2), 63–90. http://dx.doi.org/10.1016/0079-6611(86)90007-8.

Mariotti A., Germon J. C., Hubert P., Kaiser P., Letolle R., Tardieux A. and Tardieux P. (1981) Experimental determination of nitrogen kinetic isotope fractionation: some principles; illustration for the denitrification and nitrification processes. *Plant Soil* **62**, 413–430.

Matsumoto K. and Sarmiento J. L. (2008) A corollary to the silicic acid leakage hypothesis. *Paleoceanography* **23**(PA2203). http://dx.doi.org/10.1029/2007PA001515.

Milligan A. J., Varela D. E., Brzezinski M. A. and Morel F. M. M. (2004) Dynamics of silicon metabolism and silicon isotopic discrimination in a marine diatom as a function of pCO_2. *Limnol. Oceanogr.* **49**(2), 322–329. http://dx.doi.org/10.4319/lo.2004.49.2.0322.

Morley D. W., Leng M. J., Mackay A. W., Sloane H. J., Rioual P. and Battarbee R. W. (2004) Cleaning of lake sediment samples for diatom oxygen isotope analysis. *J. Paleolimnol.* **31**(3), 391–401. http://dx.doi.org/10.1023/B:JOPL.0000021854.70714.6b.

Müller P. J. and Schneider R. (1993) An automated leaching method for the determination of opal in sediments and particulate matter. *Deep Sea Res.* **40**(3), 425–444. http://dx.doi.org/10.1016/0967-0637(93)90140-X.

Nelson D. M., Goering J. J. and Boisseau D. W. (1981) Consumption and regeneration of silicic acid in three coastal upwelling systems. In *Coastal Upwelling* (ed. F. A. Richards). American Geophysical Union, pp. 242–256.

Nozaki Y. and Yamamoto Y. (2001) Radium 228 based nitrate fluxes in the eastern Indian Ocean and the South China Sea and a silicon-induced "alkalinity pump" hypothesis. *Global Biogeochem. Cycles* **15**(3), 555–567.

Pennington J. T., Mahoney K., Kuwahara V. S., Kolber D. D., Calienes R. and Chavez F. P. (2006) Primary production in the eastern tropical Pacific: a review. *Prog. Oceanogr.* **69**(2–4), 285–317. http://dx.doi.org/10.1016/j.pocean.2006.03.012.

Penven P., Echevin V., Pasapera J., Colas F. and Tam J. (2005) Average circulation, seasonal cycle, and mesoscale dynamics of the Peru Current System: a modeling approach. *J. Geophys. Res.* **110**(C10021), 1–21. http://dx.doi.org/10.1029/2005JC002945.

Ragueneau O., Savoye N., Del Amo Y., Cotten J., Tardiveau B. and Leynaert A. (2005) A new method for the measurement of biogenic silica in suspended matter of coastal waters: using Si:Al ratios to correct for the mineral interference. *Cont. Shelf Res.* **25**(5–6), 697–710. http://dx.doi.org/10.1016/j.csr.2004.09.017.

Rein B., Lückge A., Reinhardt L., Sirocko F., Wolf A. and Dullo W.-C. (2005) El Niño variability off Peru during the last 20,000 years. *Paleoceanography* **20**(PA4003), 1–18. http://dx.doi.org/10.1029/2004PA001099.

Reynolds B. C., Frank M. and Halliday A. N. (2006) Silicon isotope fractionation during nutrient utilization in the North Pacific. *Earth Planet. Sci. Lett.* **244**(1–2), 431–443. http://dx.doi.org/10.1016/j.epsl.2006.02.002.

Reynolds B. C., Aggarwal J., André L., Baxter D. C., Beucher C. P., Brzezinski M. A. and Engström E., et al. (2007) An inter-laboratory comparison of Si isotope reference materials. *J. Anal. At. Spectrom.* **22**(5), 561–568. http://dx.doi.org/10.1039/b616755a.

Reynolds B. C., Frank M. and Halliday A. N. (2008) Evidence for a major change in silicon cycling in the subarctic North Pacific at 2.73 Ma. *Paleoceanography* **23**(PA4219). http://dx.doi.org/10.1029/2007PA001563.

Robinson R. S., Martinez P., Pena L. D. and Cacho I. (2009) Nitrogen isotopic evidence for deglacial changes in nutrient supply in the eastern equatorial Pacific. *Paleoceanography* **24**(PA4213). http://dx.doi.org/10.1029/2008PA001702.

Rojas de Mendiola B. (1981) Seasonal phytoplankton distribution along the Peru coast. In *Coastal Upwelling* (ed. F. Richards). American Geophysical Union, Washington, DC, pp. 345–356.

Scheidegger K. F. and Krissek L. A. (1982) Dispersal and deposition of eolian and fluvial sediments off Peru and northern

Chile. *Geol. Soc. Am. Bull.* **93**(2), 150–162. http://dx.doi.org/10.1130/0016-7606(1982) 93 < 150.

Schrader H. (1992) Coastal upwelling and atmospheric CO_2 changes over the last 400,000 years: Peru. *Mar. Geol.* **107**(4), 239–248. http://dx.doi.org/10.1016/0025-3227(92)90074-R.

Schrader H. and Sorknes R. (1991) Peruvian coastal upwelling: late quaternary productivity changes revealed by diatoms. *Mar. Geol.* **97**, 233–249.

Shemesh A., Mortlock R. A., Smith R. J. and Froelich P. N. (1988) Determination of Ge/Si in marine siliceous microfossils: separation, cleaning and dissolution of diatoms and radiolaria. *Mar. Chem.* **25**(4), 305–323. http://dx.doi.org/10.1016/0304-4203(88)90113-2.

Strub P. T., Mesias J. M., Montecino V., Rutllant J. A. and Salinas S. (1998) Coastal ocean circulation off western South America. In *The Sea*, vol. 11 (eds. A. R. Robinson and K. H. Brink). John Wiley, Holboken, NJ, pp. 273–314.

Thiede J. and Suess E. (1983) *Coastal Upwelling: Its Sediment Record*. Plenum Publishing Corporation, New York, p. 610.

Toggweiler J. R., Dixon K. and Broecker W. S. (1991) The Peru Upwelling and the Ventilation of the South Pacific Thermocline. *J. Geophys. Res.* **96**(C11), 20467–20497. http://dx.doi.org/10.1029/91JC02063.

Tréguer P., Nelson D. M., van Bennekom A. J., DeMaster D. J., Leynaert A. and Quéguiner B. (1995) The silica balance in the world ocean: a reestimate. *Science* **268**, 375–379. http://dx.doi.org/10.1126/science.268.5209.375.

van Bennekom A. J., Berger G. W., van der Gaast S. J. and de Vries R. T. P. (1988) Primary productivity and the silica cycle in the Southern Ocean (Atlantic sector). *Palaeogeogr. Palaeoclimatol. Palaeoecol.* **67**(1–2), 19–30. http://dx.doi.org/10.1016/0031-0182(88)90120-4.

van Bennekom A. J., Jansen J. H. F., van der Gaast S. J., van Iperen J. M. and Pieters J. (1989) Aluminium-rich opal: an intermediate in the preservation of biogenic silica in the Zaire (Congo) deep-sea fan. *Deep Sea Res.* **36**(2), 173–190. http://dx.doi.org/10.1016/0198-0149(89)90132-5.

van Bennekom A. J., Buma A. G. J. and Nolting R. F. (1991) Dissolved aluminium in the Weddell-Scotia Confluence and effect of Al on the dissolution kinetics of biogenic silica. *Mar. Chem.* **35**(1–4), 423–434. http://dx.doi.org/10.1016/S0304-4203(09)90034-2.

van Cappellen P. and Qiu L. (1997) Biogenic silica dissolution in sediments of the Southern Ocean. I. Solubility. *Deep Sea Res.* **44**(5), 1109–1128. http://dx.doi.org/10.1016/S0967-0645(96)00113-0.

Varela D. E., Pride C. J. and Brzezinski M. A. (2004) Biological fractionation of silicon isotopes in Southern Ocean surface waters. *Global Biogeochem. Cycles* **18**(GB1047). http://dx.doi.org/10.1029/2003GB002140.

Winkler L. W. (1888) Die Bestimmung des im Wasser gelösten Sauerstoffs. *Ber. Dtsch. Chem. Ges.* **21**, 2843–2855.

Associate editor: James McManus